arXiv:0810.1875v1 [hep-ph] 10 Oct 2008

October 2008

Neutralino Dark Matter in an SO(10) Model with Two-step Intermediate Scale Symmetry Breaking

Manuel Drees* and Ju Min Kim†

Physikalisches Institut der Universität Bonn, Nussallee 12, 53115 Bonn, Germany

Abstract

We consider a supersymmetric Grand Unified Theory (GUT) based on the gauge group $SO(10)$ suggested by Aulakh et al., which features two–step intermediate symmetry breaking, $SO(10) \to SU(4)_C \times SU(2)_L \times SU(2)_R \to SU(3)_C \times U(1)_{B-L} \times SU(2)_L \times SU(2)_R \to SU(3)_C \times SU(2)_L \times U(1)_Y$. $45, 54, 126 + \overline{126}$ dimensional representations of Higgs superfields are employed to achieve this symmetry breaking chain. We also introduce a second, very heavy, pair of Higgs doublets, which modifies the Yukawa couplings of matter fields relative to minimal $SO(10)$ predictions. We analyze the differences in the low energy phenomenology compared to that of mSUGRA, assuming universal soft breaking scalar masses, gaugino masses and trilinear couplings at the GUT scale. We find that thermal neutralino Dark Matter remains viable in this scenario, although for small and moderate values of $\tan\beta$ the allowed region is even more highly constrained than in mSUGRA, and depends strongly on the the light neutrino masses.

*drees@th.physik.uni-bonn.de
†juminkim@th.physik.uni-bonn.de

1 Introduction

Grand Unified Theories (GUTs) based on the gauge group $SO(10)$ [1, 2] have been investigated extensively. This choice of gauge group has several appealing features. First of all, it has room for a right-handed neutrino per generation in the 16–dimensional irreducible spinor representation which includes all known matter fields. Thus it provides a beautiful explanation of the smallness of the neutrino mass via the "seesaw mechanism" [3]. Moreover, the existence of very massive right–handed neutrinos might also allow to explain the asymmetry between matter and antimatter in the Universe by thermal leptogenesis [4]. Furthermore, $SO(10)$ contains the "Pati–Salam" [5] group $SU(4)_C \times SU(2)_L \times SU(2)_R$ as subgroup, meaning that parity is preserved at high energy and broken spontaneously.

On the other hand, the fact that the rank of $SO(10)$ is five causes some complications. Recall that the rank of the Standard Model (SM) gauge group $G_{\rm SM} = SU(3)_C \times SU(2)_L \times U(1)_Y$ is only four. There are several ways of breaking $SO(10)$ down to $G_{\rm SM}$, depending on which representations of Higgs fields are introduced in the theory. Here we consider the possibility of having intermediate phase(s) at energy scales well below the GUT scale. The existence of a scale near 10^{14} GeV can be motivated by neutrino oscillation experiments [6, 7, 8]: the mass of the heaviest neutrino cannot be less than $\sqrt{\delta m^2_{atm}} \sim 0.04$ eV. In the seesaw mechanism this translates into an upper bound on the right–handed Majorana neutrinos mass if we assume that the largest neutrino Yukawa coupling is order unity, $M_N \lesssim 10^{14}$ GeV. Note that M_N breaks the $SU(2)_R$ subgroup of $SO(10)$. It thus seems natural to assume the left–right symmetric subgroup of $SO(10)$ to be broken to $G_{\rm SM}$ near this scale ("M_R"), if we assume that the Yukawa coupling that gives rise to the Majorana mass M_N is also of order unity.

In this work, we will analyze the consequences of this assumption, by considering the low energy phenomenology of a supersymmetric $SO(10)$ model suggested by Aulakh et al. [9]. It features the symmetry breaking chain

$$SO(10) \xrightarrow[M_X]{54} G_{422D} \xrightarrow[M_C]{45} G_{3122} \xrightarrow[M_R]{126+\overline{126}} G_{\rm SM}\,. \tag{1}$$

Here we have used the notation $G_{3122} = SU(3)_C \times U(1)_{B-L} \times SU(2)_R \times SU(2)_L$ and $G_{422D} = SU(4)_C \times SU(2)_R \times SU(2)_L \times D$, where D is a discrete symmetry which ensures that $SU(2)_L$ and $SU(2)_R$ have equal gauge couplings. We assume universal ("mSUGRA" [10]) boundary conditions for the soft supersymmetry breaking terms at the GUT scale M_X. This means that all soft breaking scalar masses are equal to m_0 at the GUT scale, while all gaugino masses are equal to $M_{1/2}$; moreover, all SUSY breaking trilinear scalar couplings are characterized by the single parameter A_0.

Introducing two intermediate scales, and the corresponding additional gauge, matter and Higgs superfields, has three main effects. First, the right–handed neutrinos obtain Majorana masses at scale M_R by coupling to the **126**–dimensional Higgs whose vacuum expectation value (VEV) is responsible for breaking G_{3122} in Eq.(1). These Majorana Yukawa couplings, as well as the extra Dirac couplings of the light neutrinos, will change the low energy spectrum of soft breaking parameters via renormalization group equations (RGEs). Secondly, since we have to introduce many more additional Higgs than gauge superfields to achieve the symmetry breaking chain (1), all gauge couplings increase quite rapidly at high energy scales $\gtrsim M_R$. As a result the gaugino masses, which we assume to be universal at M_X, decrease significantly when they evolve down to M_R. Finally, the enhanced gauge symmetry at energies $\gtrsim M_R$ also increases the size of gauge contributions to the RGE of all scalar masses. Note that the second

and third effect tend to cancel, if the scalar masses are expressed in terms of the GUT–scale input parameter m_0 and $M_{1/2}$.

The rest of this paper is organized as follows. In the next Section, we review the main features of the model [9] we are considering. We also describe the numerical methods used in our analysis. In Sec. 3 we discuss the most important experimental and cosmological constraints on the parameter space of the model. Our numerical results are given in Sec. 4. Special attention is devoted to the regions of parameter space where the lightest neutralino makes a good thermal Dark Matter candidate in standard cosmology. Finally, we conclude in Sec. 5.

2 The Set-Up

2.1 The model

We will consider the model suggested by Aulakh et al. [9]. It is based on the gauge group $SO(10)$. Besides three generations of matter superfields residing in **16**–dimensional representations as well as the **45**–dimensional gauge superfields, we introduce Higgs superfields in the **54, 45, 126**, $\overline{\mathbf{126}}$ and **10** representations of $SO(10)$. The Higgs superfields required to break $SO(10)$ down to $G_{\rm SM}$ can be described by the tensors

$$\begin{aligned}
\mathbf{54} &: S_{ij} = S_{ji} \text{ and } S_{ii} = 0\,, \quad \mathbf{45} : A_{ij} = -A_{ji}\,, \\
\mathbf{126} &: \Sigma_{ijklm} = \frac{i}{5!}\epsilon_{ijklmopqrs}\Sigma_{opqrs}\,, \\
\overline{\mathbf{126}} &: \overline{\Sigma}_{ijklm} = -\frac{i}{5!}\epsilon_{ijklmopqrs}\overline{\Sigma}_{opqrs}
\end{aligned} \tag{2}$$

where the subscripts $i, j, k, \ldots$ run from 1 to 10, and repeated subscripts are summed.

This allows us to realize the symmetry breaking chain (1) with a purely renormalizable superpotential, given by [9]

$$W_{SSB} = \frac{m_S}{2}{\rm tr}S^2 + \frac{\lambda_S}{3}{\rm tr}S^3 + \frac{m_A}{2}{\rm tr}A^2 + \lambda{\rm tr}A^2S + m_\Sigma\Sigma\overline{\Sigma} + \eta_S\Sigma^2S + \overline{\eta}_S\overline{\Sigma}^2S + \eta_A\Sigma\overline{\Sigma}A\,. \tag{3}$$

A crucial observation [11, 9] is that some components of the Higgs superfields listed in (2) are much lighter than one might naively expect. For example, even though the **45**–plet A is responsible for the breaking of G_{422D} to G_{3122} at scale M_C, some components of A only acquire masses of order M_C^2/M_X or M_R^2/M_C, whichever is larger. Similarly, even though Σ and $\overline{\Sigma}$ are responsible for breaking G_{3122} to the SM gauge group, some of their components only get masses of order M_R^2/M_X. On the other hand, some components of A, Σ and $\overline{\Sigma}$ obtain masses of order M_X.

This is summarized in Table 1. Here we have used the decompositions of the Higgs fields under $SU(4)_C \times SU(2)_L \times SU(2)_R$:

$$\begin{aligned}
S &= (1,1,1) \oplus (20,1,1) \oplus (1,3,3) \oplus (6,2,2)\,; \\
A &= (15,1,1) \oplus (1,1,3) \oplus (1,3,1) \oplus (6,2,2)\,; \\
\overline{\Sigma} &= (10,1,3) \oplus (\overline{10},3,1) \oplus (15,2,2) \oplus (6,1,1)\,; \\
\Sigma &= (\overline{10},1,3) \oplus (10,3,1) \oplus (15,2,2) \oplus (6,1,1)\,.
\end{aligned} \tag{4}$$

The components of the Higgs fields that acquire large vacuum expectation values (vevs) appear as the first term in each right–hand side (rhs) of Eqs.(4); in addition, the $(1,1,3)$ component of A is also assumed to obtain a nonzero vev [9].

State	Mass
all of S all of A, except $(15,1,1)_A$ all of Σ and $\overline{\Sigma}$, except $SU(4)_C$ (anti–)decuplets	$\sim M_X$
$(\overline{10},3,1)_{\overline{\Sigma}}$ and $(10,3,1)_{\Sigma}$ color triplets and sextets of $(10,1,3)_{\overline{\Sigma}}$ and $(\overline{10},1,3)_{\Sigma}$ color triplets of $(15,1,1)_A$	$\sim M_C$
$(\delta^0 - \overline{\delta}^0), \quad \delta^+, \quad \overline{\delta}^-$	$\sim M_R$
color octet and singlet of $(15,1,1)_A$	$\sim M_1 \equiv \max\left[\frac{M_R^2}{M_C}, \frac{M_C^2}{M_X}\right]$
$(\delta^0 + \overline{\delta}^0), \quad \delta^{++}, \quad \overline{\delta}^{--}$	$\sim M_2 \equiv M_R^2/M_X$

Table 1: The spectrum of Higgs superfields after symmetry breaking. The Higgs superfields have been introduced in Eq.(2), and their decomposition into irreducible representations of $SU(4)_C \times SU(2)_L \times SU(2)_R$ is given in Eq.(4). $\delta^{0,+,++}$ form the color singlet part of the $(\overline{10},1,3)$ component of Σ, while $\bar{\delta}^{0,-,--}$ form the color singlet part of $(10,1,3)$ of $\overline{\Sigma}$. Adapted from ref.[9].

We also need Higgs superfields in the **10**–dimensional representation of $SO(10)$ to provide the Higgs doublet superfields of the Minimal Supersymmetric Standard Model (MSSM) that break the electroweak gauge symmetry. Minimal $SO(10)$, with a single **10**, would require all Yukawa couplings of one generation to unify, which leads to wrong predictions for ratios of quark and lepton masses.* Introducing G_{422D} as symmetry group between M_X and M_C aggravates this problem, since it predicts Yukawa unification at scale M_C if both MSSM Higgs doublets reside in a single **(1,2,2)** of $SU(4)_C \times SU(2)_L \times SU(2)_R$. We therefore include two such superfields. We assume that the additional bidoublet obtains a mass through the coupling to the $(1,3,1)$ of A, in which case its mass will be of order $M_2 = M_R^2/M_X$ [9].

Let us discuss the structure of the matter Yukawa couplings in a bit more detail. Here we are only interested in third generation couplings, which can be large enough to affect the weak–scale sparticle spectrum significantly. The Yukawa unification conditions we will derive will not work for first and second generation fermions. We assume that this problem is solved by introducing some more complicated flavor structures, e.g. via non–renormalizable terms, without introducing additional large couplings.

At energy scales below M_2 we have the well–known MSSM superpotential,

$$W_{\rm Yuk,MSSM} = Y_u U^c Q H_u + Y_d D^c Q H_d + Y_e E^c L H_d \,, \tag{5}$$

where Q and L are the quark and lepton doublets, U^c, D^c and E^c the corresponding singlets, and H_u and H_d the two Higgs doublet superfields. In Eq.(5) we have suppressed all generation and group indices.

*This prediction can be made to work for the third generation, if the ratio of MSSM Higgs vevs $\tan\beta$ is large and sfermion masses lie well above a TeV [12]; however, they will fail for the first two generations.

At energies above M_2 the second pair of Higgs doublets as well as some parts of the $SU(2)$ triplet Higgs superfields (see Table 1) become accessible. A general ansatz for the matter superpotential is then

$$W_{\rm Yuk,gen} = \sum_{i=1}^{2} \left(Y_{u,i} U^c Q H_{u,i} + Y_{d,i} D^c Q H_{d,i} + Y_{e,i} E^c L H_{d,i} \right) + \frac{1}{2} Y_N E^c \bar{\delta}^{--} E^c \,. \tag{6}$$

The last term in Eq.(6) results from the interaction giving rise to large Majorana masses for the right–handed neutrino superfields (see below). The light Higgs doublets H_u, H_d are mixtures of the Higgs superfields appearing in Eq.(6):

$$\begin{aligned} H_u &= \cos\varphi_u H_{u,1} + \sin\varphi_u H_{u,2} \,; \\ H_d &= \cos\varphi_d H_{d,1} + \sin\varphi_d H_{d,2} \,. \end{aligned} \tag{7}$$

At scales above M_R, U^c and D^c form a doublet Q^c of $SU(2)_R$; similarly, the right–handed neutrino superfield N^c and E^c form an $SU(2)_R$ doublet L^c.[†] Moreover, the Higgs superfields $H_{u,i}$, $H_{d,i}$ are grouped into two bidoublets Φ_i. Finally, at this scale all members of the $SU(2)_R$ triplet Higgs superfield $\bar{\delta}$ become accessible. The superpotential (6) then becomes

$$W_{\rm Yuk,3122} = \sum_{i=1}^{2} \left(Y_{q,i} Q^c Q \Phi_i + Y_{l,i} L^c L \Phi_i \right) + \frac{1}{2} Y_N L^c \bar{\delta} L^c \,. \tag{8}$$

The last term in Eq.(8) gives rise to large Majorana masses for the N^c once the neutral component of the $SU(2)_R$ triplet $\bar{\delta} \in \overline{\Sigma}$ gets a vev. Finally, at scales above M_C, Q and L are unified into F in the **(4,2,1)** representation of G_{422}, while Q^c and L^c join to form F^c in the $(\overline{\mathbf{4}}, \mathbf{1}, \mathbf{2})$ representation. One is then left with a single Yukawa coupling per Higgs bidoublet,

$$W_{\rm Yuk,422} = \sum_{i=1}^{2} Y_i F^c F \Phi_i + \frac{1}{2} Y_N \left(F^c \overline{\Sigma}_R F^c + F \overline{\Sigma}_L F \right) \,, \tag{9}$$

where $\overline{\Sigma}_R$ and $\overline{\Sigma}_L$ are in the $(\mathbf{10}, \mathbf{1}, \mathbf{3})$ and $(\overline{\mathbf{10}}, \mathbf{3}, \mathbf{1})$ representation, respectively, of $SU(4)_C \times SU(2)_L \times SU(2)_R$; the last term in Eq.(9) also has to have coupling Y_N due to the discrete D symmetry.

As a first simplification, let us work in the basis where $Y_2 = 0$. This can always be accomplished by a unitary rotation between the two Φ_i. Since superpotential couplings renormalize multiplicatively, this choice is renormalization scale invariant. It is then easy to see that, through the matching conditions at M_C, $Y_{q,2} = Y_{l,2} = 0$ in Eq.(8); similarly, matching at scale M_R implies $Y_{u,2} = Y_{d,2} = Y_{e,2} = 0$ in Eq.(6). The sums in Eqs.(6) and (8) thus also collapse to single terms. Inserting Eqs.(7) into Eq.(6) then leads to the following matching conditions for the MSSM Yukawa couplings at scale M_2:

$$Y_{u,1} = Y_u / \cos\varphi_u \,; \quad Y_{d,1} = Y_d / \cos\varphi_d \,; \quad Y_{e,1} = Y_e / \cos\varphi_d \,. \tag{10}$$

We can get phenomenologically acceptable couplings only if $\varphi_u \neq \varphi_d$.

Note that the high–scale couplings $Y_{f,1}$ are always larger than or equal to the low–scale (MSSM) couplings Y_f ($f = u, d, e$). On the other hand, we know that in the MSSM the top

[†]Note that Q^c and L^c are independent left–chiral superfields, *not* the charge conjugates of Q and L.

Yukawa coupling is already fairly close to its upper bound imposed by the requirement that it remains perturbative up to very large scales. Eq.(10) therefore implies that $|\cos\varphi_u| \simeq 1$. For definiteness we therefore set

$$\cos\varphi_u = 1\,, \tag{11}$$

i.e. $\varphi_u = 0$. This minimizes $Y_{u,1}$; we will see shortly that it also minimizes all other MSSM matter Yukawa couplings above scale M_2. These couplings appear with positive signs on the right–hand side of the RGE for the new coupling Y_N. The choice (11) therefore maximizes the upper bound on $Y_N(M_R)$ that can be derived from the requirement that this coupling remains perturbative up to M_X. We will see below that this in turn minimizes the lower bound on the mass of the light physical neutrino for fixed M_R.

Eq.(8) implies that $Y_{u,1}(M_R) = Y_{d,1}(M_R) \equiv Y_{q,1}(M_R)$. This is compatible with Eqs.(10) and (11) only for

$$\cos\varphi_d = \frac{Y_d(M_2)}{Y_u(M_2)}\left[\frac{g_1^2(M_R)}{g_1^2(M_2)}\right]^{1/60}\quad; \tag{12}$$

the last factor in Eq.(12) accounts for the different RGE running of $Y_{u,1}$ and $Y_{d,1}$ caused by the different hypercharges of the U^c and D^c superfields. Since this factor is quite close to unity, Eqs.(10)–(12) imply that $Y_{d,1}$ and $Y_{u,1}$ are very similar. Since even in the MSSM the bottom and tau Yukawa couplings become similar at large energy scales, Eq.(12) implies that all third generation Yukawa couplings will be comparable to the top Yukawa coupling at all scales above M_2. In the given framework this is inescapable, unless we introduce additional heavy superfields which mix with the MSSM matter fields.

At the $SU(4)_C$ breaking scale $Y_{q,1}$ and $Y_{l,1}$ are unified into the single coupling Y_1. The unification of the bottom and top coupling can always be achieved through an appropriate choice of φ_d; however, the unification of the bottom and tau Yukawa couplings is a nontrivial constraint. This prediction is similar to that of minimal $SU(5)$. In a scenario without intermediate scales, the tau Yukawa coupling at scale M_X is typically a bit larger than the bottom coupling. In our case unification should happen at $M_C < M_X$, which reduces the difference between the two couplings at their putative unification scale. On the other hand, above the scale $M_1 < M_C$ the $SU(3)_C$ coupling is larger in our scenario than in the MSSM. This increases the RG running of Y_b. The two effects largely cancel. As a result, we find that $Y_\tau(M_C)$ exceeds $Y_b(M_C)$ by typically 10 to 20%. We blame this on threshold effects – Table 1 shows that quite a few new fields attain masses of order M_C – and/or on the additional physics required to reproduce masses and mixing angles of the lighter SM fermions. As a practical matter, we set

$$Y_1(M_C) = \frac{Y_{l,1}(M_C) + Y_{q,1}(M_C)}{2}\,. \tag{13}$$

The superpotential (8) generates neutrino masses through the celebrated ("type I") see–saw formula [3],[‡]

$$m_\nu = \frac{m_D^2}{M_N} = \frac{(Y_{l,1}\langle H_u^0\rangle)^2}{Y_N\langle\overline{\sigma}\rangle}\,. \tag{14}$$

Here $\overline{\sigma} \in (\overline{\mathbf{10}}, \mathbf{1}, \mathbf{3}) \in \overline{\Sigma}$ is the neutral component of the $SU(2)_R$ triplet Higgs boson.[§] Note that the neutrino Dirac Yukawa coupling is related to that of charged leptons by $SU(2)_R$,

[‡]Note that there is no quartic scalar coupling which could lead to a "type II" seesaw contribution.

[§]The field $\bar{\delta}^0$ listed in Table 1 is the physical remnant of $\overline{\sigma}$ after $G_{3122} \to G_{\rm SM}$ symmetry breaking.

which in turn is related to the (top) quark Yukawa coupling by $SU(4)_C$ symmetry, as described above. We assume here that the Y_N are (mildly) hierarchical, so that only the third generation coupling is large enough to effect the weak–scale spectrum significantly via the RGE.

For given $M_R = \langle\overline{\sigma}\rangle$ and light neutrino mass m_ν, Eq.(14) can then be used to determine the value of Y_N at the GUT scale. We vary m_ν between 0.2 and 0.4 eV. Note that smaller values of m_ν lead to a *larger* coupling Y_N.

The occurrence of fields that are not part of the MSSM at mass scales well below M_R is crucial. As well known, in the MSSM all three gauge couplings (almost) meet at an energy scale near $2 \cdot 10^{16}$ GeV [13]. Without additional fields that are lighter than M_R it would not be possible to modify the running of the gauge couplings such that intermediate scales, and hence energy ranges where the symmetry group is larger than $G_{\rm SM}$ but smaller than the GUT group, can occur. We will analyze the running of the gauge couplings in more detail in Sec. 4.

We will see in Sec. 4 that the lightest new particles, with mass $M_2 \sim M_R^2/M_X$, are still much too heavy to directly lead to visible effects at collider or rare decay experiments. Nevertheless their existence affects the renormalization group equations (RGE) describing the running of the masses of all superparticles and Higgs bosons. The one–loop RGE for Yukawa couplings and soft breaking parameters that hold for different ranges of energies are listed in the Appendix. In order to compare with the frequently studied [14] mSUGRA or cMSSM scenario, we assume universal boundary conditions, as already noted in the Introduction.

2.2 The numerical calculation

The RGE listed in the Appendix are too complicated to allow an analytical solution. Instead, we incorporated them into the code `SOFTSUSY2.0` [15]. This program computes the weak–scale MSSM spectrum by iteratively solving the RGE, starting from universal boundary conditions for the soft breaking parameters. An iterative treatment is necessary since many parameters are fixed at the weak scale, rather than the GUT scale. These include the three (MS)SM gauge couplings, the masses of SM matter fermions[¶], the mass of the Z boson, and the ratio $\tan\beta$ of vevs of the two MSSM Higgs bosons. We use one–loop RGE throughout, but include important weak–scale threshold corrections; these are known to change the physical masses of third generation fermions significantly, in particular at large $\tan\beta$ [16]. Note that the program implements radiative breaking of the electroweak gauge symmetry [17], again including important weak–scale threshold corrections.

At the intermediate scales M_1, M_2, M_R and M_C (some of) the RGE have to be changed. In the discussion of Yukawa couplings we described how to pick the appropriate high–scale couplings, given the low–energy couplings. This procedure is applicable when going from low to high energies. When going in the opposite direction, we use the same matching conditions, employing the values of $\cos\varphi_d$ and the ratio of $Y_{l,1}(M_C)/Y_{q,1}(M_C)$ determined from the previous RG running from low to high energies to fix the values of low–scale Yukawa couplings. The matching of gauge couplings and soft breaking terms directly follows from the group structure, and will be discussed in Sec. 4.1 and in the Appendix, respectively

The output of `SOFTSUSY` is passed on to the program `micrOMEGAs 1.3.7` [18], which computes the Dark Matter (DM) relic density as well as the BR($b \to s\gamma$) and δa_μ, the anomalous magnetic moment of the muon (see below).

[¶]Only the masses of third generation fermions are kept, since the Yukawa couplings in the first and second generation are too small to significantly affect the evolution of the sparticle masses.

3 Accelerator and Cosmological Constraints

In this Section we describe the constraints we impose on the model.

3.1 Electroweak symmetry breaking and tachyons

As mentioned earlier, electroweak symmetry breaking (EWSB) is incorporated into `SOFTSUSY`. Technically, it solves equations that allow to express μ^2 and the bilinear Higgs soft mass parameter $B\mu$ in terms of M_Z and the ratio of vevs $\tan\beta$. However, these equations sometimes formally lead to $\mu^2 < 0$, which indicates that EWSB is not possible for the given set of input parameters. For reasons that will become clear shortly, here we are mostly interested in solutions with large $\tan\beta$. In this case EWSB is possible iff the (properly threshold corrected) value of the squared soft breaking mass of the up–type Higgs boson at the weak scale is negative, $m^2_{H_u}(M_{\rm SUSY}) < 0$.

3.2 Constraints from collider searches

As in mSUGRA, the most important constraints are those on the masses of the lightest Higgs boson and the lightest chargino. In combination, they imply that constraints on the masses of strongly interacting sparticles [19] are automatically satisfied.

We interpret the limit $M_{H_{\rm SM}} > 114.4$ GeV, which comes from searches for $e^+e^- \to ZH^0$, as imposing a lower mass on the mass of the lighter CP–even Higgs boson of the MSSM,

$$M_h > 111 \text{ GeV}\,, \tag{15}$$

where we allowed for a ~ 3 GeV theoretical uncertainty [20] in the calculation of m_h. We also require

$$m_{\tilde{\chi}_1^\pm} > 104 \text{ GeV}\,, \tag{16}$$

since scenarios allowing chargino masses significantly below the highest LEP beam energy cannot be realized in our scenario: these scenarios all require the presence of sneutrinos with mass near or slightly below that of the chargino, and scenarios where both the sneutrino and $\tilde{\chi}_1^\pm$ have mass below the limit (16) violate the Higgs constraint (15).

3.3 Branching ratio of $b \to s\gamma$

In the SM, flavor changing neutral currents (FCNC) are absent at tree level. Thus, the radiative $B \to X_s\gamma$ decay is mediated by loops containing up–type quarks and W bosons. As well known [21], SUSY loop contributions can be comparable to those from the SM. Therefore, the measurement of the branching ratio for this decay, performed by CLEO, Belle and BaBar [22],

$$B(b \to s\gamma) = (355 \pm 24^{+9}_{-10} \pm 3) \times 10^{-6} \tag{17}$$

can be used to constrain the parameter space of our model. The first error in (17) includes statistical, systematic, extrapolation and $b \to d\gamma$ contamination errors, while the last two are estimated to be the difference of the average after varying the central value of each experimental result by $\pm 1\sigma$. To be conservative, we take the linear sum of the errors, since the calculation strongly depends on the assumptions of the boundary conditions. Even minor deviations from

strict universality, for example due to the running between M_X and M_{Pl} [23, 24], can have very large effects [25] .

As mentioned above, we used `micrOMEGAs 1.3` [18] to calculate the branching ratio. Therein, minimal flavor violation (i.e. the only source of flavor violation at the weak scale is in the CKM matrix) is assumed [26]; hence only contributions from charged Higgs and top quarks, and charginos and stops are included. These contributions are indeed usually by far the dominant ones if universal boundary conditions are assumed [27], as in our analysis.

3.4 The anomalous magnetic moment of the muon

The anomalous magnetic moment of the muon is one of the most precisely calculated and measured quantities. There is an about 3σ discrepancy between the SM prediction based on data from e^+e^- annihilation into hadrons and the experimental value. While this is still somewhat controversial – an SM prediction which instead makes use of τ decay data plus some assumptions is in fair agreement with the data – we here want to investigate the parameter space of our model that allows to explain this discrepancy.

The world average, dominated by data from the E821 collaboration at BNL, is [19]

$$a_\mu^{exp} = \frac{g_\mu - 2}{2} = (1165920.80 \pm 0.63) \times 10^{-9} \,. \tag{18}$$

The theoretical value [28] is calculated as the sum of (i) pure QED contributions including the diagrams of virtual photon, vacuum polarization (VP) from e, μ and τ, and leptonic light–by–light scattering, (ii) hadronic contributions including VP from quarks, most reliably estimated using $e^+e^- \to$ hadrons data, and hadronic light–by–light scattering, and (iii) electroweak contributions. The resulting SM prediction is [19]

$$a_\mu^{theory} = (1165919.52 \pm 0.52) \times 10^{-9} \,. \tag{19}$$

Demanding that supersymmetric loops, involving smuons and neutralinos or smuon neutrinos and charginos, lead to agreement between theory and experiment at the 2σ level thus implies

$$4.6 \times 10^{-10} < \delta a_{\mu,\mathrm{SUSY}} < 21.0 \times 10^{-10} \,. \tag{20}$$

We use `micrOMEGAs` to calculate $\delta a_{\mu,\mathrm{SUSY}}$.

3.5 Dark Matter relic density

We assume that all cosmological Dark Matter (DM) consists of lightest neutralinos. This implies that $\tilde{\chi}_1^0$ has to be the lightest superparticle (LSP); this imposes a constraint on the parameter space of our model.

Far more important is the requirement that the thermal $\tilde{\chi}_1^0$ relic density, calculated using `micrOMEGAs` under the usual assumptions of the minimal cosmological model [29], reproduces the value derived from the WMAP 3-year data [30] and other observations pertaining to structure formation in the universe:

$$0.097 < \Omega_{\mathrm{DM}} h^2 < 0.113, \quad \text{at } 68\% \text{ CL} \,. \tag{21}$$

Here Ω_{DM} is the DM mass density in units of the critical (closure) density, and h is the Hubble constant in units of 100 km/(s·Mpc). As we will see below, this provides the most stringent

constraint on the parameter space. This is not surprising, given the small size of the error bars in (21).*

4 Results

We are now ready to present some results. We begin with an analysis of the running of the gauge couplings, which determines the values of our intermediate scales. We then discuss analytical results for first and second generation sfermion as well as gaugino masses, before analyzing the ratios of (s)particle masses that are most relevant for the calculation of the DM relic density. We will conclude this Section with a survey of the parameter space of the model.

For the top quark mass, we have taken $m_t = 170.9$ GeV, as has recently been measured at the Tevatron [32].

4.1 RG Analysis of the gauge couplings

The current world averages of the gauge coupling constants at scale M_Z are [19]:

$$\alpha_1(M_Z) = 0.01695, \quad \alpha_2(M_Z) = 0.03382, \quad \alpha_3(M_Z) = 0.1176\,. \tag{22}$$

Note that we use GUT normalization for the $U(1)$ gauge coupling, i.e. our α_1 exceeds the hypercharge coupling α_Y in its usual normalization by a factor of 5/3. The values of these couplings at different energies are determined by RGE; to one–loop order, these can be written as

$$\frac{d\alpha_i}{dt} = -\frac{\alpha_i}{2\pi} b_i, \quad (i = 1, 2, 3)\,. \tag{23}$$

Here $t = \ln(Q/Q_0)$, where Q_0 is some reference energy scale. Note the minus sign in Eq.(23); in this convention, a positive b_i corresponds to an asymptotically free gauge coupling. The values of the b_i depend on which particles are "active" at a given energy scale Q; in the usual step function approximation of integrating out heavy particles, we treat all particles with masses $< Q$ to be (fully) active at scale Q.

This leads to the values of the b_i listed in Table 2, which we adapted from ref.[9]. Note that we list the coefficients that allow to describe the running of the three factor groups of the SM gauge group. The $SU(2)_L$ factor remains independent up to scale M_X, i.e. the third column of Table 2 always describes the running of the coupling of an $SU(2)$ group. Recall that above M_C, $SU(2)_L$ and $SU(2)_R$ have the same coupling, since the discrete symmetry D is exact; the coefficient $b_2^{(5)}$ therefore also describes the running of the $SU(2)_R$ coupling. Moreover, at scale M_C the strong interactions get embedded into $SU(4)_C$, with boundary condition $g_3(M_C) = g_4(M_C)$. The coefficient $b_3^{(5)}$ therefore describes the running of the $SU(4)_C$ gauge coupling, which is the same as the running of the coupling of the $SU(3)_C$ subgroup of $SU(4)_C$ at $Q \geq M_C$.

The fate of the $U(1)_Y$ factor of $G_{\rm SM}$ is a bit more complicated. At scale M_R it gets embedded into $SU(2)_R \times U(1)_{B-L}$, with matching condition $\alpha_1^{-1} = 2/(5\alpha_{B-L}) + 3/(5\alpha_{2R})$. The $U(1)_{B-L}$ factor in turn gets absorbed into $SU(4)_C$ at scale M_C, i.e. $\alpha_{B-L}(M_C) = \alpha_4(M_C)$. Although the hypercharge coupling is thus "spread" over two different gauge couplings for $Q \geq M_R$, its running can still be described by Eq.(23), with coefficient listed in Table 2.

*Recently the WMAP 5 year data have been released [31]. The resulting range for $\Omega_{\rm DM}h^2$ is very similar to that of Eq.(21).

Table 2: The coefficients of the beta functions of the gauge couplings of the SM gauge group, valid at different energy scales Q.

Energy range	$b_1^{(k)}$	$b_2^{(k)}$	$b_3^{(k)}$
$M_Z < Q < M_S$	$-41/10$	$19/6$	7
$M_S < Q < M_2$	$-33/5$	-1	3
$M_2 < Q < M_R$	-12	-2	3
$M_R < Q < M_1$	$-48/5$	-2	3
$M_1 < Q < M_C$	$-48/5$	-2	0
$M_C < Q < M_X$	$-194/5$	-42	-34

Eqs.(22) and (23), together with the coefficients $b_i^{(k)}$ listed in Table 2, allow us to predict the values of the gauge couplings at all $Q \geq M_Z$. Of course, the three gauge couplings of the (MS)SM are supposed to meet at scale M_X in our model. This leads to two independent constraints. On the other hand, the intermediate scale M_R and M_C are free parameters of our model; the scales M_1 and M_2 are derived quantities, as described in Table 1. For given value of M_X the two independent unification conditions can thus be solved for M_R and M_C. The running of any one of the three (MS)SM gauge couplings can then be used to determine the value of the $SO(10)$ gauge coupling α_U. Notice that this procedure will work for any assumed value of M_X, i.e. it still leaves one parameter undetermined. We refer the reader to ref.[9] for a further discussion of the unification condition, including explicit solutions of the RGE of the gauge couplings.

In Fig. 1 we show one–loop predictions for the intermediate scales M_R and M_C, as well as the value of M_X, as function of $1/\alpha_U$. We see that smaller values of M_X correspond to larger

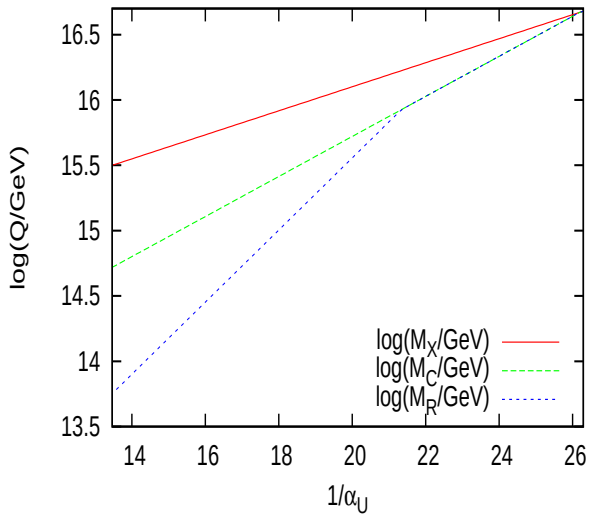

Figure 1: The values of the intermediate scales M_R and M_C, as function of the inverse of the $SO(10)$ coupling α_U. Here we took $M_S = 1$ TeV as sparticle mass scale.

values of α_U. The reason is that decreasing M_X increases the ratios M_X/M_R and M_X/M_C. Table 2 shows that all b_i are large and negative for $Q > M_C$; recall that this corresponds to gauge couplings increasing with energy. A large M_X/M_R means that these beta–functions are valid over a large range of energies, leading to a large value of α_U. On the other hand, proton decay through dimension 6 operators conservatively requires $M_X \geq 3 \cdot 10^{15}$ GeV. Fig. 1 shows that this corresponds to $\alpha_U \simeq 1/13.5$, safely in the perturbative region (significantly smaller than $\alpha_3(M_Z)$, for example).

Since the purpose of our paper is to study the influence of the intermediate scales on the low–energy spectrum, we take this minimal value of M_X as our default choice. The intermediate scales are then found at

$$M_R = 10^{13.75} \text{ GeV}\,, \quad M_C = 10^{14.72} \text{ GeV}\,. \tag{24}$$

Increasing M_X reduces the impact of the intermediate scales. At $M_X \simeq 10^{15.8}$ GeV, corresponding to $\alpha_U \simeq 1/21$, the scales M_R and M_C coincide. When M_X is increased to about $10^{16.6}$ GeV, M_C in turn coincides with M_X. At that point no intermediate scales are left, i.e. this limit reproduces the usual MSSM. Higher values of M_X are not possible. By varying M_X between $10^{15.5}$ GeV and $10^{16.6}$ GeV we can thus smoothly turn on the intermediate scales and study their impact on weak–scale physics.

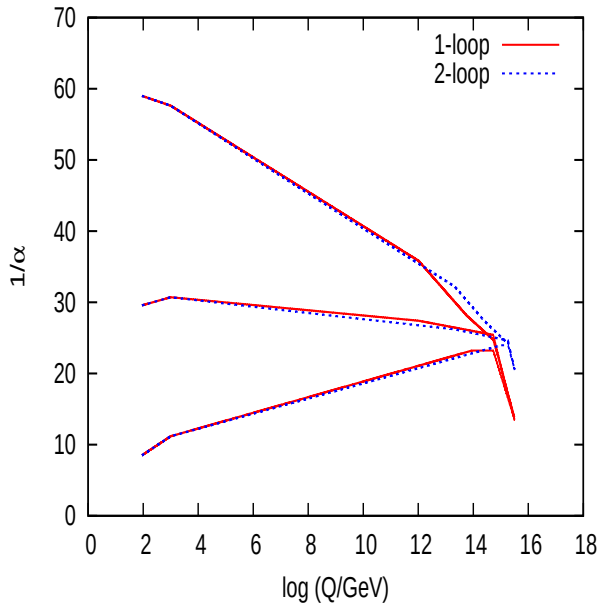

Figure 2: The running inverse gauge couplings α_i^{-1}. The curves at the top [middle, bottom] are for the $U(1)_Y$ [$SU(2)_L$, $SU(3)_C$] couplings. Solid and dashed curves show results for one– and two–loop RGE, respectively.

The rapid increase of the gauge couplings at $Q \geq M_C$ can also be seen in Fig.2, which shows the running of the gauge couplings as function of the energy scale for our default set of parameters. The solid lines show the predictions from the one–loop RGE we have used so far, whereas the dashed curves are based on two–loop RGE [33] (ignoring, however, the subdominant contributions from Yukawa couplings to the running of the gauge couplings). Evidently using two–loop RGE increases the intermediate scales for this value of M_X, making

the model more mSUGRA–like. However, an analysis based on two–loop RGE should also treat the (rather numerous, in our case) threshold corrections more carefully. So far we have assumed that all (s)particles whose masses are of the order of a given scale, as listed in Table 1, have *exactly* that mass. This will not be true in many cases. However, the exact masses will depend on many unknown couplings describing interactions of these superheavy fields. A proper treatment of threshold corrections would therefore introduce many new free parameters. Since threshold and two–loop effects are generically of similar magnitude [33], we assume that there are combinations of parameters where an analysis including two–loop and threshold effects leads to similar results as the one–loop analysis. The use of one–loop beta functions has the practical advantage that the equations determining M_R and M_C can easily be solved analytically [9].

4.2 Analytical results

At the one–loop level, the gaugino masses evolve in the same way as the squared gauge couplings do. Therefore, the ratios of weak–scale gaugino masses are the same as in mSUGRA, i.e. $M_1 : M_2 : M_3 \simeq 1 : 2 : 6$.* This follows from the fact that the three MSSM gauge couplings are identical at M_X, and have their measured values (22) at scale M_Z. These ratios are therefore independent of the intermediate scales.

However, for fixed $M_{1/2}$ the weak–scale gaugino masses are now much smaller than in mSUGRA, since the ratios $\alpha_i(M_Z)/\alpha_U$ are much smaller, as shown in Fig. 2. Writing

$$M_i(M_{\rm SUSY}) = c_i M_{1/2} \quad (i = 1\,, 2\,, 3)\,, \tag{25}$$

we have

$$c_1 \simeq 0.23\,, \quad c_2 \simeq 0.46\,, \quad c_3 \simeq 1.4\,, \tag{26}$$

for $M_{\rm SUSY} \sim 1$ TeV; these are nearly two times smaller than the corresponding coefficients in mSUGRA [10].

The RGE for the masses of first and second generation sfermions, whose Yukawa couplings are negligible, can also be solved analytically [10]. Writing†

$$m^2_{\tilde f}(M_{\rm SUSY}) = m_0^2 + c_{\tilde f} M^2_{1/2}\,, \tag{27}$$

we have

$$c_{\tilde e_R} \simeq 0.15\,, \quad c_{\tilde l_L} \simeq 0.21\,, \quad c_{\tilde q} \simeq 1.16\,. \tag{28}$$

Here $\tilde e_R$ and $\tilde l_L$ stands for $U(1)_Y$ singlet and doublet sleptons, respectively, while $\tilde q$ stands for an average first or second generation squark; as in mSUGRA, $SU(2)_L$ doublet squarks are slightly heavier than singlet squarks. We checked that the analytical and numerical calculations of $m^2_{\tilde e_R}$ match within 0.1%. Note that the coefficient $c_{\tilde e_R}$ is numerically almost the same as in mSUGRA [10]. This is due to a cancellation of two effects. On the one hand, $\tilde e_R$ is a non–singlet under both $SU(2)_R$ and $SU(4)_C$, giving rise to new gauge contributions to its mass at scales above M_R and M_C, respectively, which increase $c_{\tilde e_R}$. On the other hand, we saw that

*These are running masses. The on–shell masses differ by weak–scale threshold corrections [16], which are included in `SOFTSUSY`.

†The running weak–scale sfermion masses also receive small $D-$term contributions, which we omit in the following discussion, but include in the numerical analysis. In addition, the physical (pole) masses again differ from the running masses by threshold corrections [16], which are included in `SOFTSUSY`.

for fixed $M_{1/2}$ the gaugino masses at scales $Q < M_X$ are smaller than in mSUGRA, which reduces all $c_{\tilde{f}}$. The latter effect is dominant for all fields that transform non–trivially under either $SU(2)_L$ or $SU(3)_C$. As a result, the mass difference between $SU(2)_L$ singlet and doublet sleptons is significantly smaller than in mSUGRA; recall that the $SU(2)_L$ doublet sleptons are singlets under $SU(2)_R$.

Note that if we apply the universal boundary conditions at some energy scale $Q > M_X$, the sfermion masses obtain additional contributions due to $SO(10)$ gauge interactions. These increase the values of all $c_{\tilde{f}}$ by the same amount, since all sfermions reside in the **16** of $SO(10)$; this additional contribution would thus be relatively most important for $\tilde{e}_R$ [34]. However, since we need large Higgs representations to realize the breaking chain (1), the $SO(10)$ gauge coupling α_U hits a Landau pole soon after the unification scale [9]. Hence we expect some new, possibly strongly interacting, physics to occur just above M_X. The range of energies where $SO(10)$ RGE are applicable is therefore probably quite small.

From Eqs.(25)–(28) we can derive lower bounds on the ratios of sfermion to gaugino masses. Of particular interest for the calculation of the Dark Matter relic density is the relation

$$\frac{m_{\tilde{e}_R}(M_{\rm SUSY})}{|M_1|(M_{\rm SUSY})} \gtrsim 1.68\,. \tag{29}$$

In mSUGRA, the lower bound, which is saturated for $M_{1/2}^2 \gg m_0^2$, is instead slightly below unity. This is important, since it implies that for fixed m_0 and increasing $M_{1/2}$, one will eventually reach a gaugino mass such that $m_{\tilde{e}_R} = m_{\tilde{\chi}_1^0}$, leading to strong $\tilde{\chi}_1^0 - \tilde{e}_R$ co–annihilation. The bound (29) implies that this never happens in our scenario. However, as in mSUGRA the lighter $\tilde{\tau}$ mass eigenstate $\tilde{\tau}_1$ can be significantly lighter than $\tilde{e}_R$.[‡] We will see later that $\tilde{\chi}_1^0 - \tilde{\tau}_1$ co–annihilation remains possible in our model. However, Eq.(29) already indicates that the parameter space where this can happen is (even) more limited than in mSUGRA.

Our model also predicts

$$\frac{m_{\tilde{l}_L}(M_{\rm SUSY})}{|M_2(M_{\rm SUSY})|} \gtrsim 1\,, \tag{30}$$

which means that $\tilde{\chi}_2^0$ and $\tilde{\chi}_1^\pm$ decays into $SU(2)_L$ doublet sleptons will be strongly suppressed. In contrast, in mSUGRA $SU(2)_L$ doublet sleptons can be some 15% lighter than $SU(2)_L$ gauginos. On the other hand, the bound

$$\frac{m_{\tilde{q}}(M_{\rm SUSY})}{|M_3(M_{\rm SUSY})|} \gtrsim 0.77 \tag{31}$$

is very similar to that in mSUGRA. It still leaves room for two–body decays of gluinos into first or second generation squarks.

4.3 Mass ratios

In this section we show numerical results for some (ratios of) masses that are important for the determination of the thermal $\tilde{\chi}_1^0$ relic density. We focus on masses whose weak–scale values are affected by the potentially large Yukawa couplings in the theory. We saw in Sec. 2.1 that all third generation Yukawa couplings involving Higgs doublets are quite large at energies

[‡]For this reason, usually the most important co–annihilation channel is $\tilde{\chi}_1^0 - \tilde{\tau}_1$ co–annihilation [35]: scenarios giving $m_{\tilde{\chi}_1^0} = m_{\tilde{e}_R}$ are already excluded, since here $\tilde{\tau}_1$ would be the LSP.

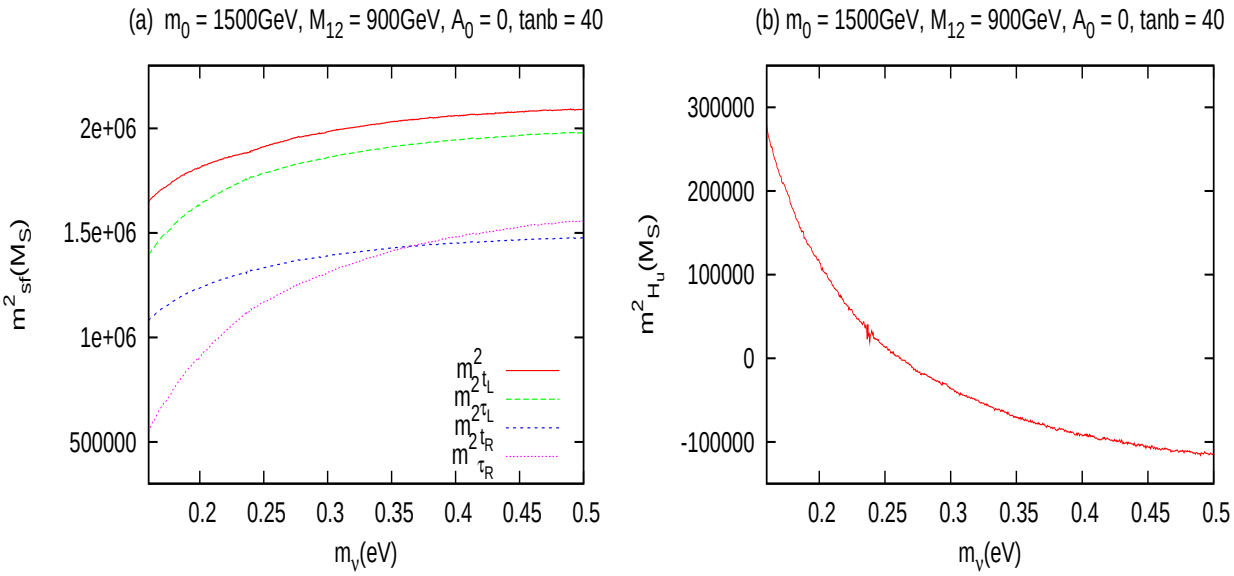

Figure 3: Squared weak–scale running masses in GeV^2 of (a) $\tilde{t}$ and $\tilde{\tau}$ sfermions and (b) the up–type Higgs boson, as function of the neutrino mass. The other input parameters are: $m_0 = 1.5$ TeV, $M_{1/2} = 0.9$ TeV, $A_0 = 0$, $\tan\beta = 40$ and $\mu > 0$.

$\geq M_2$; at energies $\geq M_R$ this includes the new neutrino Yukawa coupling Y_ν, which is equal to that of the charged lepton by $SU(2)_R$ invariance. The coupling Y_N, which determines the Majorana masses of the heavy neutrinos, can also be sizable. Recall that Y_N is related to the light neutrino mass and $M_R = \langle\bar{\sigma}\rangle$ through Eq.(14).

Yukawa couplings tend to reduce weak–scale scalar masses for fixed m_0 and $M_{1/2}$. Y_N begins to act – on the mass of $\tilde{\tau}_R$ – at scale M_2; at the same scale, the bottom and tau couplings become large even if $\tan\beta$ is not large, see Eq.(12). At energies above M_R the neutrino coupling Y_ν becomes active, reducing the weak–scale masses of $\tilde{\tau}_L$ and of the Higgs boson H_u. Above M_C, all weak–scale third generation sfermion masses will be reduced by Y_N. We therefore expect the difference between first and third generation weak–scale sfermion masses to be larger than in mSUGRA. This effect should be strongest for $\tilde{\tau}_R$ and $\tilde{\tau}_L$. The reduction should be more pronounced at small and moderate $\tan\beta$, since for large $\tan\beta$ all third generation Yukawa couplings are sizable even in the MSSM.

This is illustrated in the left frame of Fig. 3, which shows the dependence of the soft–breaking masses of $\tilde{t}_L$, $\tilde{t}_R$, $\tilde{\tau}_L$ and $\tilde{\tau}_R$ as a function of the mass m_ν of the heaviest light neutrino. Recall that this mass is proportional to $1/Y_N$, i.e. smaller m_ν correspond to larger Y_N, and hence to smaller weak–scale sfermion masses.

On the other hand, the right frame in Fig. 3 shows that the running soft breaking mass of the Higgs bosons with positive hypercharge *in*creases with decreasing m_ν. We just saw that larger values of Y_N reduce $m^2_{\tilde{t}_L}$ and $m^2_{\tilde{t}_R}$ at all energies below M_X. This reduces the term $\propto Y_t^2$. Since this term drives $m^2_{H_u}$ to smaller or even negative values, reducing its size leads to an increase of the weak–scale value of $m^2_{H_u}$. Recall that $m^2_{H_u}(M_{\rm SUSY}) < 0$ is required to achieve electroweak symmetry breaking with $\tan\beta \gg 1$. This figure therefore implies that the parameter space permitting radiative breaking of the $SU(2) \times U(1)_Y$ symmetry will be smaller for smaller values of m_ν.

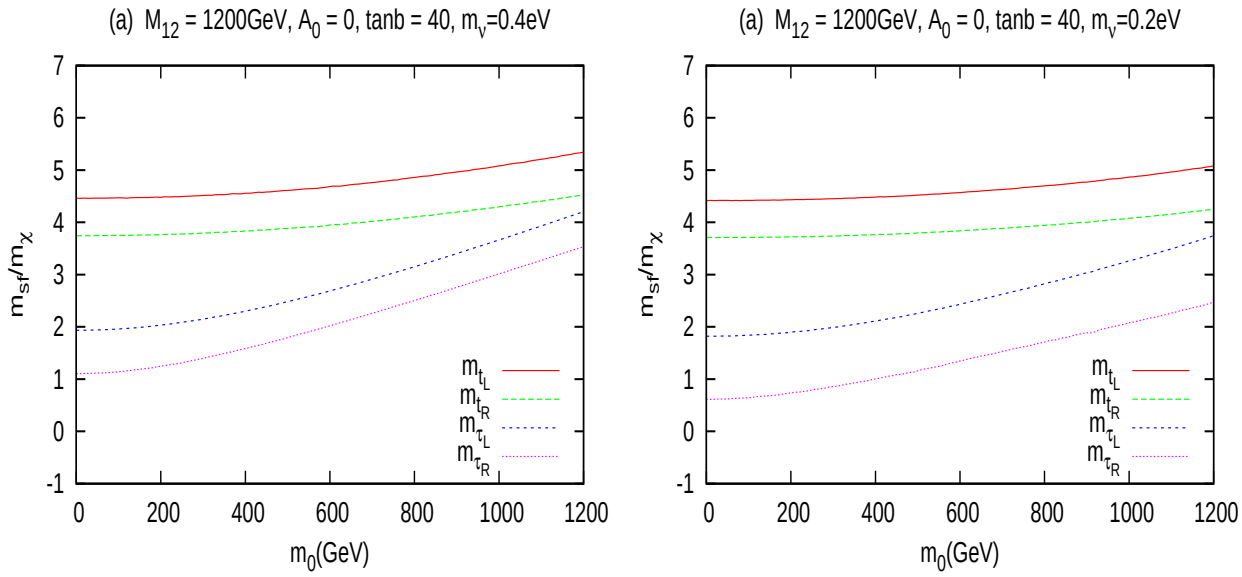

Figure 4: The ratio of third generation sfermion masses to the mass of the lightest neutralino as function of m_0, for $m_\nu = 0.4$ eV (left), $m_\nu = 0.2$ eV (right). The values of the other input parameters are $M_{1/2} = 1.2$ TeV, $A_0 = 0$, $\tan\beta = 40$ and $\mu > 0$.

The Yukawa coupling Y_N also reduces the value of the soft breaking mass of $\bar{\Sigma}$, whose vev is responsible for the masses of the heavy neutrinos, and contributes to the $SU(2)_R \times U(1)_{B-L} \to U(1)_Y$ breaking. Since this occurs at a scale $M_R \gg M_{\rm SUSY}$, we introduced a field Σ, which permits to keep the $SU(2)_R$ and $U(1)_{B-L}$ $D-$terms much below M_R^2. However, since $Y_N \neq 0$ implies $m^2_{\bar{\Sigma}}(M_R) < m^2_{\Sigma}(M_R)$, $\langle\Sigma\rangle < \langle\bar{\Sigma}\rangle$. Since $\langle\bar{\Sigma}\rangle^2 - \langle\Sigma\rangle^2 \propto (m^2_{\Sigma} - m^2_{\bar{\Sigma}}) \propto M^2_{\rm SUSY}$ [36], this effect does not spoil the hierarchy $M_R \gg M_{\rm SUSY}$, but it does give new non–vanishing contributions to the masses of sfermions and Higgs bosons. However, they are subdominant for most of the parameter space, partly due to the small splitting between M_R and M_C, and partly because m^2_{Σ} and $m^2_{\bar{\Sigma}}$ receive identical, large gauge contributions, in particular for $Q > M_C$ where Σ and $\bar{\Sigma}$ are embedded in (anti–)decuplets of $SU(4)_C$. In fact, we found that the ratio $(m^2_{\Sigma} - m^2_{\bar{\Sigma}})/m^2_{\Sigma}$ is, at most, a few %. Hence, these new $D-$term contributions can be ignored.

Fig. 4 shows the dependence of the ratios $m_{\tilde{t}_{L,R}}/m_{\tilde{\chi}^0_1}$ and $m_{\tilde{\tau}_{L,R}}/m_{\tilde{\chi}^0_1}$, taken at scale $Q = M_{\rm SUSY}$, on m_0. For $m_0^2 \ll M^2_{1/2}$ the stop squarks are significantly heavier than the stau sleptons. This qualitative behavior is the same as for first and second generation squarks, see Eq.(28). On the other hand, if $m_0 \gtrsim M_{1/2}$ and relatively small Y_N (left frame), $m_{\tilde{t}_R}$ can be smaller than $m_{\tilde{\tau}_{L,R}}$, since the top Yukawa coupling is significantly larger than that of the τ lepton.

The right frame of Fig. 4 shows that increasing Y_N reduces the dependence of third generation sfermion masses on m_0. In fact, for $m_\nu = 0.2$ eV we observe a sort of "focus point" [37] for $m_{\tilde{t}_R}$, i.e. $m_{\tilde{t}_R}(M_{\rm SUSY})$ becomes almost independent of m_0. This implies that there is *no* focus point behavior of $m^2_{H_u}(M_{\rm SUSY})$, i.e. this soft breaking parameter, which largely determines electroweak symmetry breaking for $\tan^2\beta \gg 1$, does depend on m_0. Hence large values of m_0 will not be "natural" (by the definition employed in refs.[37]) if Y_N affects the weak–scale third generation masses significantly.

The scalar masses shown in Fig. 4 are running masses at scale $M_{\rm SUSY}$. The physical masses

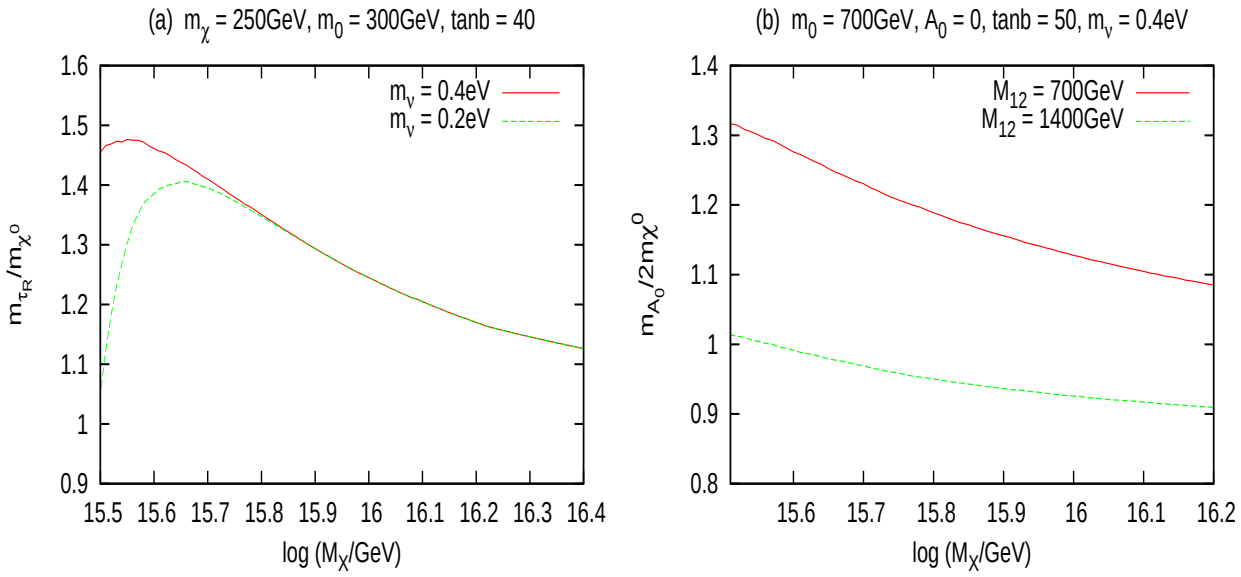

Figure 5: The ratio of $m_{\tilde{\tau}_R}$ to $m_{\tilde{\chi}^0}$ (left), $m_{\tilde{A}^0}$ to $2m_{\tilde{\chi}^0}$ (right), as the unification scale M_X is varied. Recall that this implies corresponding variations of the intermediate scales M_C and M_R, see Fig. 1.

will be affected by threshold corrections and, more importantly for third generation sfermions, by mixing between $SU(2)$ singlets and doublets. This mixing reduces the mass of the lighter eigenstates $\tilde{\tau}_1$ and $\tilde{t}_1$, so that $m_{\tilde{\tau}_1} < \min(m_{\tilde{\tau}_L}, m_{\tilde{\tau}_R})$ and similar for $m_{\tilde{t}_1}$. Nevertheless Fig. 4 shows that co–annihilation will usually only be possible with $\tilde{\tau}_1$. This is similar to mSUGRA. Note, however, that Fig. 4 is for $\tan\beta = 40$. Recall that co–annihilation with first or second generation sfermions is not possible here, see Eq.(29). Moreover, comparison of the two frames of Fig. 4 shows that the effects of Y_N on the $\tilde{\tau}$ masses are quite small if $m_0^2 \ll M_{1/2}^2$. As a result, we find that $\tilde{\tau}$ co–annihilation is possible in our model only for $\tan\beta \gtrsim 27$.

The left frame of Fig.5 illustrates the dependence of the ratio $m_{\tilde{\tau}_R}/m_{\tilde{\chi}^0}$ on the GUT scale. Recall that for $M_X = 10^{16.4}$ GeV our model becomes indistinguishable from mSUGRA, as far as the weak–scale spectrum is concerned. As discussed in the previous Subsection, in the absence of new large Yukawa couplings this ratio can only become larger as the intermediate scale is turned on. However, we saw in Fig.4 that the Majorana Yukawa coupling Y_N does give a large positive contribution to the RGE of $m_{\tilde{\tau}_R}$, reducing its weak–scale value. These two effects clearly compete with each other. We see that even a rather large Y_N, corresponding to $m_{\nu_\tau} = 0.2$ eV, can change $m_{\tilde{\tau}_R}(M_{\rm SUSY})$ significantly only if $M_X < 10^{15.8}$ GeV; recall from Fig. 1 that this corresponds to the region of parameter space where $M_R < M_C$. In this case the possibility to have $\tilde{\tau}_1$ co–annihilation obviously strongly depends on m_{ν_τ}.

The right frame of Fig.5 shows the ratio $m_{A^0}/2m_{\tilde{\chi}^0}$. This ratio needs to be close to unity for $\tilde{\chi}_1^0$ annihilation through $s-$channel A^0 exchange to be enhanced. We see that reducing M_X, i.e. turning on the intermediate scales, slightly increases this ratio even if Y_N is small. For given m_0, this can be compensated by increasing $M_{1/2}$. We thus expect the "$A-$funnel" region to survive in our scenario, if $\tan\beta \gtrsim 50$ and for small Y_N. Increasing Y_N will increase $m_A(M_{\rm SUSY})$; this is analogous to the increase of $m_{H_u}^2$ depicted in the right frame of Fig. 3.

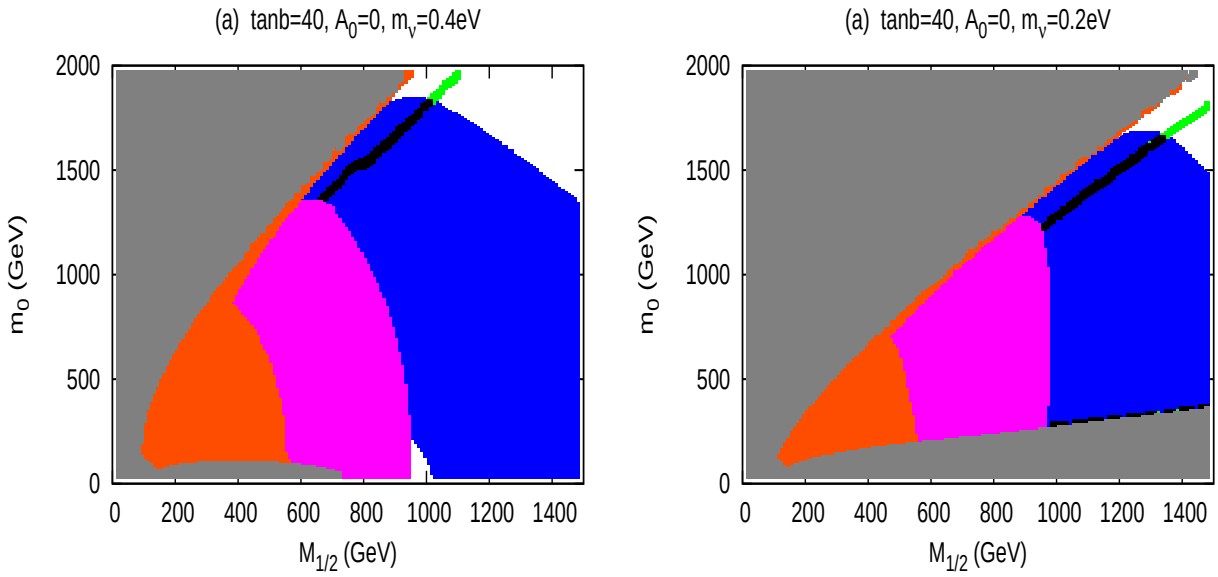

Figure 6: Constraints on the $(m_0, M_{1/2})$ plane of our model. The grey areas are those excluded by the EWSB condition or by tachyonic or too light sfermions. The region excluded by the Higgs and chargino mass constraints is shown in bright red and the own excluded by the $b \to s\gamma$ constraint in pink. The blue area satisfies the $g_\mu - 2$ constraint (20), while green regions satisfy the Dark Matter constraint (21). Finally, black regions satisfy all constraints.

4.4 Regions of the $(m_0,\ M_{1/2})$ plane

In this Subsection, we show the $(m_0, M_{1/2})$ plane of our model, indicating the regions where the various accelerator as well cosmological constraints discussed in Sec. 3 are satisfied. We scan the parameter space only up to $(m_0, M_{1/2}) = (2000\text{ GeV}, 1500\text{ GeV})$. Even larger sparticle masses appear quite unnatural. The LHC should be able to probe the entire parameter space we show [38]; recall that $M_{1/2} = 1.5$ TeV corresponds to a gluino mass around 2 TeV in our scenario. We focus on large values of $\tan\beta$. We saw in the previous subsection that this is required both for the $A-$funnel and the for $\tilde{\tau}$ co–annihilation region in our scenario. Finally, sign(μ) is chosen positive in all plots, in accordance with the indication of an additional positive contribution to g_μ; recall also that taking $\mu > 0$ makes it easier to satisfy the $b \to s\gamma$ constraint [27].

A first example, for $A_0 = 0$ and $\tan\beta = 40$, is presented in Fig. 6; the left (right) frame is for small (large) coupling Y_N. The grey regions are mostly excluded by the requirement of correct electroweak symmetry breaking; in the right frame the region of small m_0 is instead excluded because $\tilde{\tau}_1$ is too light (below either the LEP limit or the mass of $\tilde{\chi}_1^0$). As expected from the discussion of Fig. 3, this region is considerably larger for large Y_N.

The bright red regions are excluded by the chargino search limit (16) or by the limit (15) on the mass of the lightest CP–even Higgs boson; the latter is relevant for $M_{1/2} \lesssim 500$ GeV, while the former excludes the narrow red strip bordering the grey region at large m_0 and large $M_{1/2}$. Finally, the pink regions are excluded by the constraint (17) on the branching ratio for radiative b decays. Some supersymmetric contributions to the corresponding amplitude grow $\propto \tan\beta$. This constraint therefore becomes relevant at the large values of $\tan\beta$ required to realize $\tilde{\tau}$ co–annihilation and/or the $A-$funnel in our model.

Turning to observables that require a non–vanishing contribution from supersymmetric particles, in the blue regions the constraint (20) from the anomalous magnetic moment of the muon is satisfied. The corresponding diagrams are quite similar to those contributing to $b \to s\gamma$ decays. In particular, some contributions again grow $\propto \tan\beta$. As in mSUGRA [14], we find regions of the parameter space at sufficiently large $M_{1/2}$ where electroweak gauginos and sleptons are sufficiently light to give a sizable positive contribution to g_μ, while (stop) squarks are sufficiently heavy not to reduce the branching ratio for $b \to s\gamma$ decays too much.

Note that the red, pink and blue regions all extend to much larger values of $M_{1/2}$ than in mSUGRA [14]. The reason is that the corresponding constraints probe weak–scale (s)particle masses; we saw in Eqs.(25)–(28) that a given $M_{1/2}$ corresponds to much lighter gauginos and sfermions in our scenario than in mSUGRA. Moreover, we saw in Figs. 3 and 4 that the additional large Yukawa couplings in our model tend to reduce weak–scale stop masses. They also increase $m^2_{H_u}$, which leads to a reduction of $|\mu|$ via the condition of electroweak symmetry breaking. Both effects, which become more important for smaller m_ν, increase the absolute size of the stop–chargino loop contribution to $b \to s\gamma$ decays. This has to be compensated by increasing m_0 and/or $M_{1/2}$. The $b \to s\gamma$ constraint is therefore relatively more important in our scenario than in mSUGRA, especially if Y_N is sizable.

Note also that the region excluded because it does not permit radiative symmetry breaking has a pronounced slope even for the larger neutrino mass, i.e. smaller coupling Y_N. This shows that $m^2_{H_u}(M_{\rm SUSY})$ has significant dependence on m_0, as remarked earlier, i.e. there is no focusing behavior of this parameter. As expected from our discussion of Fig. 3, this upper bound on m_0 becomes stronger when Y_N is increased, i.e. when m_ν is decreased. In a strip close to this excluded region we nevertheless expect the lightest neutralino to have a large, perhaps dominant, higgsino component; this region will therefore have a somewhat similar phenomenology as the "focus point" region in mSUGRA [37], especially as far as Dark Matter is concerned.

Finally, in the narrow green strips the constraint (21) on the Dark Matter relic density is satisfied; these strips would obviously look broader if we had indicated the 2σ allowed region, as more commonly done. The overlap between the DM– and $g_\mu-$allowed regions is colored in black.

In Fig. 6 we find two such regions. At small m_0 $\tilde\chi^0_1$ is bino–like, and achieves a sufficiently small relic density through co–annihilation with $\tilde\tau_1$. For small Y_N (left frame) this region is strongly constrained by the bound on $b \to s\gamma$ decays. We saw in Fig. 4 that increasing Y_N reduces the $\tilde\tau$ masses, making it possible to find scenarios with $m_{\tilde\tau_1} \simeq m_{\tilde\chi^0_1}$ even if $M_{1/2}$ is large.

We just saw that for values of m_0 not far below the upper bound imposed by electroweak symmetry breaking, $\tilde\chi^0_1$ has a sizable higgsino component. For some range of parameters it achieves the correct relic density mostly through annihilation into channels involving weak gauge bosons. As in mSUGRA, this second DM–allowed region extends to very large values of m_0 and $M_{1/2}$, with $\tilde\chi^0_1$ becoming increasingly higgsino–like (and therefore co–annihilation with $\tilde\chi^0_2$ and $\tilde\chi^\pm_1$ becoming increasingly important [39].)

As in mSUGRA, $\tan\beta = 40$ is not large enough to allow $m_A \simeq 2m_{\tilde\chi^0_1}$ if $\mu > 0$. Fig. 7 shows that this "$A-$pole" region becomes accessible for $\tan\beta = 50$. Sufficiently small values of m_A are only possible if the soft breaking mass $m^2_{H_d}$ of the second Higgs boson also becomes negative (and large) at the weak scale. We saw in the discussion of Fig. 5 that decreasing m_ν will increase $m^2_{H_u}(M_{\rm SUSY})$. Indeed, in Fig. 7 we find a well–defined $A-$funnel only for $m_\nu = 0.4$ eV (left frame).

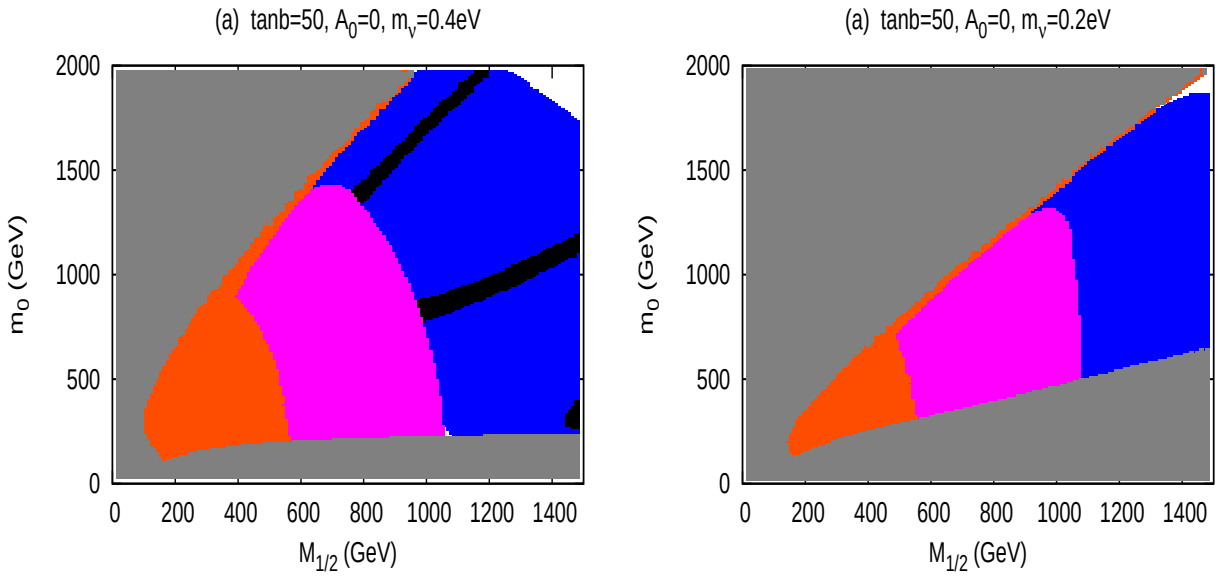

Figure 7: Constraints on the $(m_0, M_{1/2})$ plane of our model. Parameter values and color code are the same as in Fig. 6, except that $\tan\beta$ has been increased to 50.

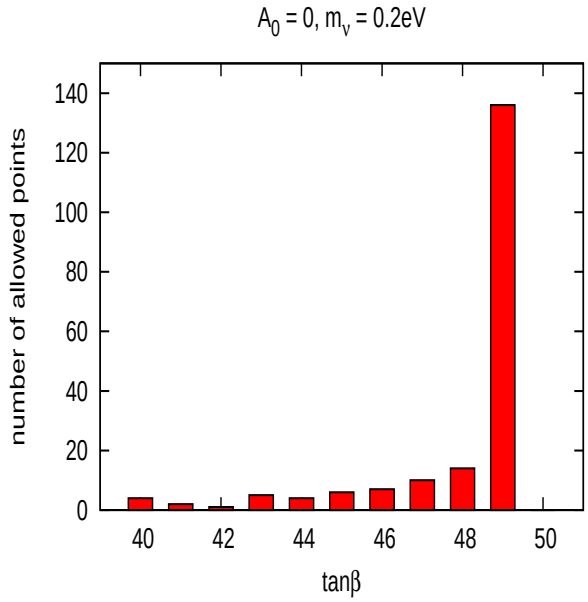

Figure 8: Number of allowed points (by all constraints) for 1TeV $< m_0 <$ 1.5TeV; 1.1TeV $< M_{1/2} <$ 1.4TeV, with the grid 25GeV. The allowed region is very large when $\tan\beta = 49$.

If we instead take $m_\nu = 0.2$ eV (right frame), we find that the $\tilde{\chi}_1^0$ relic density becomes too low in the entire allowed region of the $(m_0,\ M_{1/2})$ plane we scanned. One reason is that increasing Y_N reduces $\mu(M_{\rm SUSY})$, as discussed above. This increases the coupling of the LSP to neutral Higgs bosons, in particular to A. Since for $\tan\beta = 50$ the b and τ Yukawa couplings are quite sizable, virtual A exchange diagrams become large, even though $2m_{\tilde{\chi}_1^0}$ is somewhat below m_A. Increasing m_0 increases m_A, but at the same time decreases μ even further, and

therefore does not allow to achieve a DM relic density above the lower bound in the range (21). Moreover, recall that reducing m_ν also reduces the $\tilde{\tau}$ masses. In addition, the very large value of $\tan\beta$ considered in this figure leads to large $\tilde{\tau}_L\tilde{\tau}_R$ mixing, which allows $\tilde{\chi}_1^0\tilde{\chi}_1^0 \to \tau^+\tau^-$ annihilation through $\tilde{\tau}$ exchange even if the initial state is in an $S-$wave [40]. Finally, for $M_{1/2}$ close to its lower bound, $\tilde{\chi}_1^0\tilde{\tau}_1$ co–annihilation again becomes important. Note that this indicates that the DM-allowed region may be quite large for some $\tan\beta$ between 40 and 50, and $m_\nu = 0.2$ eV. Indeed, Fig. 8 shows that for $\tan\beta = 49$, about 50% of the points we scanned that satisfy the other constrains are also compatible with the DM constraint.

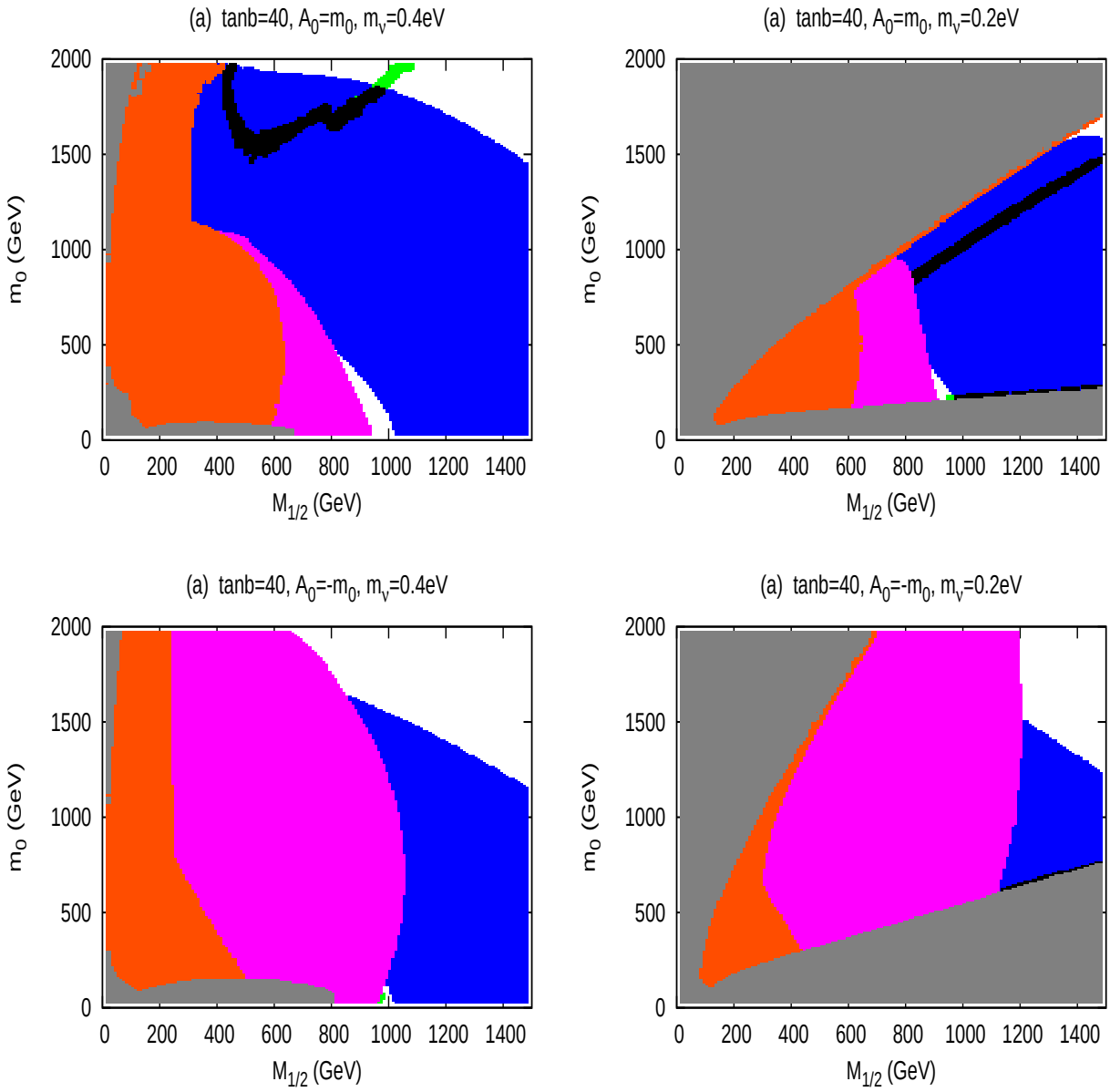

Figure 9: Constraints on the $(m_0, M_{1/2})$ plane of our model. Parameter values and color code are the same as in Fig. 6, except that we now take $A_0 = m_0$ ($A_0 = -m_0$) in the top (bottom) row.

In Fig. 9 we explore the effect of taking a non–zero value of A_0. We see that the value of A_0 can have quite a dramatic effect on the region excluded because it does not allow electroweak

symmetry breaking. This can be understood as follows. By dimensional arguments and the fact that scalar masses always appear as squares in the RGE, the soft breaking mass of the up–type Higgs boson at the weak scale can be written as

$$m_{H_u}^2(M_{\rm SUSY}) = am_0^2 + bM_{1/2}^2 + cA_0^2 + dM_{1/2}A_0\,. \tag{32}$$

The values of the coefficients a, b, c, d depend on the dimensionless couplings in the theory, as well as (logarithmically) on $M_{\rm SUSY}$. In our model, a and d are positive while b and c are negative. Hence increasing m_0 makes EWSB more difficult, while increasing $M_{1/2}$ makes it easier if $M_{1/2} > |A_0|$. This explains the qualitative feature of the regions excluded by the EWSB constraint in Figs. 6 and 7.

On the other hand, if $|A_0| \gg M_{1/2}$, increasing the absolute value of A_0 also aids EWSB independent of its sign. This explains why the region excluded by the EWSB constraint becomes much smaller in the two left frames of Fig. 9. Fig. 6 shows that, for the given small value of Y_N, the EWSB constraint only excludes scenarios with $m_0 > M_{1/2}$ even if $A_0 = 0$. In the critical region $|A_0| = m_0$ is thus always sufficiently larger than $M_{1/2}$. Finally, for given absolute value of A_0, EWSB will be easier for negative than for positive A_0. This explains why the EWSB excluded region is significantly larger in the upper–right frame of Fig. 9 than in the lower–right frame. Note also that a sizable Y_N decreases the absolute size of c, since Y_N reduces $|A_t|$ for $Q > M_C$, see Eq.(A.34)

A nonvanishing A_0 also changes the regions allowed by the other constraints. In particular, $A_0 < 0$ increase $\tilde{t}_L - \tilde{t}_R$ mixing. This has two effects. On the one hand, it increases the radiatively corrected mass of the lightest CP–even Higgs boson, thereby reducing the size of the red regions in Fig. 9. On the other hand, it increases the $\tilde{t}\tilde{\chi}^\pm$ contributions to radiative $b \to s\gamma$ decays, increasing the size of the pink regions. This latter effect completely removes the DM–allowed region close to the EWSB–forbidden region, where $\tilde{\chi}_1^0$ has sizable higgsino component. As a result, for $A_0 = -m_0$, only the small $\tilde{\tau}$ co–annihilation region survives. On the other hand, for $A_0 = m_0$ we again find sizable DM–allowed regions at large m_0; the structure in this (black) region at $M_{1/2} \simeq 800$ GeV in the top–left frame is due to the opening of the $\tilde{\chi}_1^0\tilde{\chi}_1^0 \to t\bar{t}$ channel.

5 Summary and Conclusions

Supersymmetric $SO(10)$ GUTs have become attractive extensions of the SM, especially since the observation of the nonzero neutrino mass. However, there is a small discrepancy between the order of the expected mass of the right handed neutrino in the seesaw mechanism and the GUT scale; it can be explained in a natural way if one postulates intermediate scales where the gauge symmetry is larger than that of the SM, but smaller than $SO(10)$.

Therefore, in this work we chose a model [9] which gives us intermediate symmetry breaking scale(s), and analyzed how this affects the low energy phenomenology. We found that the relation between weak–scale and GUT–scale parameters is quite different in this model than in the widely considered mSUGRA scenario. Perhaps more importantly, ratios of different weak–scale masses also differ from mSUGRA. In particular, the slepton to electroweak gaugino mass ratios are higher than in mSUGRA. As a result, co–annihilation is only possible with the lighter $\tilde{\tau}$ eigenstate, and only at large $\tan\beta$ and/or large Yukawa coupling Y_N of the SM singlet neutrinos; the latter corresponds to small values for the light neutrino masses.

Radiative electroweak symmetry breaking also is more difficult in this model than in mSUGRA. This makes it easier to find Dark Matter allowed solutions where the lightest neutralino has a significant higgsino component. As in mSUGRA, the location of this region strongly depends on A_0; in addition, we find a strong dependence on Y_N, i.e. on the light neutrino mass. We also found that for very large $\tan\beta$ and large Y_N most of the $(m_0, M_{1/2})$ plane leads to too small a $\tilde{\chi}_1^0$ relic density. As a corollary, there exist combinations of Y_N and $\tan\beta$ where $\Omega_{\rm DM}h^2$ has weak dependence on m_0 and $M_{1/2}$; however, in this case it depends strongly on $\tan\beta$ and Y_N. Finally, as in mSUGRA the $A-$pole region only exists at large $\tan\beta$; it disappears for large values of Y_N.

We would like to point it out that, even though our analysis is done for a specific model, many of our results should remain qualitatively correct for other $SO(10)$ GUT scenarios, as long as the seesaw mechanism at an intermediate scale plays a role. In particular, the relation between the right–handed stau mass and the Majorana Yukawa coupling Y_N, which largely determines the behavior of the co–annihilation region, does not depend on the details of either the symmetry breaking chain or the seesaw structure. Any partial unification above the see–saw scale also implies that Y_N will affect other sfermion masses, and hence the conditions for radiative symmetry breaking.

In summary, the model we considered relates several phenomena, and can hence be probed through a large variety of measurements, from proton decay (which imposes limits on the GUT scale) over neutrino masses and Dark Matter physics to collider physics. We intend to investigate characteristic features of this scenario at the LHC in a future publication.

Acknowledgments

JMK thanks to C. S. Aulakh and M. Kakizaki for useful discussions. This work was partially supported by the Marie Curie Training Research Network "UniverseNet" under contract no. MRTN-CT-2006-035863, as well as by the European Network of Theoretical Astroparticle Physics ENTApP ILIAS/N6 under contract no. RII3-CT-2004-506222. JMK was partially supported by the Bonn–Cologne Graduate School of Physics and Astronomy. We thank the KIAS school of physics for hospitality while part of this work was done.

A Renormalization Group Equations

In this section we list all relevant one–loop renormalization group equations explicitly. Our calculations are based on the general expressions of ref.[41]. We divide the entire energy range between the SUSY and GUT scales into five regions, with different particles participating in the RGE and different symmetry groups:

- Region I ($M_{\rm SUSY} < Q < M_2$) : $SU(3)_C \times SU(2)_L \times U(1)_Y$
- Region II ($M_2 < Q < M_R$) : $SU(3)_C \times SU(2)_L \times U(1)_Y$
- Region III ($M_R < Q < M_1$) : $SU(3)_C \times U(1)_{B-L} \times SU(2)_L \times SU(2)_R$
- Region IV ($M_1 < Q < M_C$) : $SU(3)_C \times U(1)_{B-L} \times SU(2)_L \times SU(2)_R$
- Region V ($M_C < Q < M_X$) : $SU(4)_C \times SU(2)_L \times SU(2)_R \times D$

In the following Subsections we discuss the running of the supersymmetric parameters (gauge couplings and parameters of the superpotential) and of the soft breaking parameters, respectively.

A.1 Superpotential Parameters

We begin with the parameters that preserve supersymmetry. The running of the gauge couplings is described by

$$\frac{d}{dt}g_a = \frac{1}{16\pi^2}\beta_{g_a}g_a^3 \quad \text{with} \quad \beta_{g_a} = \sum_R S(R) - 3C_a(G)\,. \tag{A.1}$$

Here $t = \ln(Q/Q_0)$, a labels the factor group, R the representation of the matter and Higgs superfields under this group, C_a is the quadratic Casimir of this group, and the Dynkin index $S(R)$ is defined by $\mathrm{Tr}(t_A t_B) = S(R)\delta_{AB}$, $t_{A,B}$ being matrix representations of the gauge group.

Our notation for a generic superpotential is

$$W = \frac{1}{6}Y^{ijk}\Phi_i\Phi_j\Phi_k + \frac{1}{2}\mu^{ij}\Phi_i\Phi_j\,. \tag{A.2}$$

The running of the parameters appearing in (A.2) is given by

$$\begin{aligned}\frac{d}{dt}Y^{ijk} &= Y^{ijp}\frac{1}{16\pi^2}\gamma^k_p + (k\leftrightarrow i) + (k\leftrightarrow j)\\ \frac{d}{dt}\mu^{ij} &= \mu^{ip}\frac{1}{16\pi^2}\gamma^j_p + (j\leftrightarrow i)\,,\end{aligned} \tag{A.3}$$

where summation over repeated indices is understood. The anomalous dimensions γ_i^j are given by

$$\gamma_i^j = \frac{1}{2}Y_{ipq}Y^{jpq} - 2\delta_i^j g_\alpha^2 C_\alpha(i). \tag{A.4}$$

In our case, the superpotential below M_X has been given in Eq.(5) for region I, in Eq.(6) for region II, in Eq.(8) for regions III and IV, and in Eq.(9) for region V. Recall that we take $Y_2 = Y_{q,2} = Y_{l,2} = Y_{u,2} = Y_{d,2} = Y_{e,2} = 0$; for the sake of simplicity we therefore suppress the superscript 1 on the Yukawa couplings in the following. These couplings are 3×3 matrices in generation space. We will write the RGE for general matrices, although we only kept third generation couplings in our numerical analysis. We use the general notation

$$\begin{aligned}\frac{d}{dt}Y_f &= \frac{1}{16\pi^2}\beta_{Y_f}\,;\\ \frac{d}{dt}\mu &= \frac{1}{16\pi^2}\beta_\mu\,,\end{aligned} \tag{A.5}$$

where f stands for any matter fermion. In the following we list these as well as the gauge beta–functions in the five different energy regions.

A.1.1 Region I

The coefficients of the gauge beta functions are

$$\beta_{g_a} = (33/5, 1, -3) \;\text{ for } a = (1_Y, 2_L, 3_C)\,, \tag{A.6}$$

where we have used GUT normalization for the $U(1)_Y$ factor. The corresponding coefficients for the MSSM Yukawa couplings are

$$\begin{aligned}
\beta_{Y_u} &= Y_u(\gamma_U^U + \gamma_{H_u}^{H_u}) + \gamma_Q^Q Y_u\,; \\
\beta_{Y_d} &= Y_d(\gamma_D^D + \gamma_{H_d}^{H_d}) + \gamma_Q^Q Y_d\,; \\
\beta_{Y_e} &= Y_e(\gamma_E^E + \gamma_{H_d}^{H_d}) + \gamma_L^L Y_e\,; \\
\beta_\mu &= \mu(\gamma_{H_d}^{H_d} + \gamma_{H_u}^{H_u})\,,
\end{aligned} \tag{A.7}$$

where

$$\begin{aligned}
\gamma_E^E &= 2Y_e^\dagger Y_e - \frac{6}{5}g_1^2\,; \\
\gamma_L^L &= Y_e Y_e^\dagger - \frac{3}{10}g_1^2 - \frac{3}{2}g_2^2\,; \\
\gamma_Q^Q &= Y_d Y_d^\dagger + Y_u Y_u^\dagger - \frac{1}{30}g_1^2 - \frac{3}{2}g_2^2 - \frac{8}{3}g_3^2\,; \\
\gamma_U^U &= 2Y_u^\dagger Y_u - \frac{8}{15}g_1^2 - \frac{8}{3}g_3^2\,; \\
\gamma_D^D &= 2Y_d^\dagger Y_d - \frac{2}{15}g_1^2 - \frac{8}{3}g_3^2\,; \\
\gamma_{H_d}^{H_d} &= \mathrm{tr}(3Y_d Y_d^\dagger + Y_e Y_e^\dagger) - \frac{3}{10}g_1^2 - \frac{3}{2}g_2^2\,; \\
\gamma_{H_u}^{H_u} &= 3\mathrm{tr}Y_u Y_u^\dagger - \frac{3}{10}g_1^2 - \frac{3}{2}g_2^2\,.
\end{aligned} \tag{A.8}$$

A.1.2 Region II

$$\beta_{g_a} = (12, 2, -3) \quad \text{for} \quad a = (1_Y, 2_L, 3_C)\,. \tag{A.9}$$

The Yukawa coupling beta functions of the MSSM matter fields have the same form as in Region I, but we need to introduce an RGE for Y_N:

$$\beta_{Y_N} = Y_N(\gamma_E^E + \gamma_{\bar{\delta}}^{\bar{\delta}}) + \gamma_E^E Y_N\,. \tag{A.10}$$

Except for γ_E^E the anomalous dimensions of the MSSM matter fields also remain form invariant, and we have to introduce an anomalous dimension for $\bar{\delta}^{--}$:

$$\begin{aligned}
\gamma_E^E &= 2Y_e^\dagger Y_e + Y_N^\dagger Y_N - \frac{6}{5}g_1^2\,; \\
\gamma_{\bar{\delta}}^{\bar{\delta}} &= \frac{1}{2}\mathrm{tr}(Y_N^\dagger Y_N) - \frac{24}{5}g_1^2\,.
\end{aligned} \tag{A.11}$$

Recall that we are now dealing with the couplings $Y_{f,1}$ ($f = u, d, e$), which are related to the MSSM couplings Y_f via Eqs.(10)–(12).

A.1.3 Region III

$$\beta_{g_a} = (15, 2, 6, -3) \quad \text{for } a = (1_{B-L}, 2_L, 2_R, 3_C)\,, \tag{A.12}$$

where we have again used GUT normalization for the $U(1)$ coupling. The effective coefficient $48/5$ for the running $U(1)_Y$ coupling listed in Table 2 is $\frac{3}{5}\cdot 6+\frac{2}{5}\cdot 15$, which follows from the matching condition $g_Y^{-2}=\frac{3}{5}g_R^{-2}+\frac{2}{5}g_{B-L}^{-2}$.

Since the underlying symmetry group is enhanced, and the matter superfields form multiplets correspondingly, their anomalous dimensions receive contributions from the heavy gauge bosons that become active in this energy range. We switch to the notation of Eq.(8), i.e. we introduce Q^c instead of U^c and D^c, while E^c and N^c are united in L^c and H_u and H_d are united in Φ. The number of independent Yukawa couplings is thus reduced to three:

$$\begin{aligned}\beta_{Y_q} &= Y_q(\gamma^{Q^c}_{Q^c}+\gamma^{\Phi}_{\Phi})+\gamma^{Q}_{Q}Y_q\,;\\ \beta_{Y_l} &= Y_l(\gamma^{N^c}_{L^c}+\gamma^{\Phi}_{\Phi})+\gamma^{L}_{L}Y_l\,;\\ \beta_{Y_N} &= Y_N(\gamma^{N}_{N}+\gamma^{\bar\delta}_{\bar\delta})+\gamma^{N}_{N}Y_N\,.\end{aligned} \tag{A.13}$$

The relevant anomalous dimensions read:

$$\begin{aligned}\gamma^{L^c}_{L^c} &= 2Y_l^\dagger Y_l+\frac{3}{2}Y_N^\dagger Y_N-\frac{3}{2}g_R^2-\frac{3}{4}g_{B-L}^2\,;\\ \gamma^{L}_{L} &= 2Y_l Y_l^\dagger-\frac{3}{2}g_2^2-\frac{3}{4}g_{B-L}^2\,;\\ \gamma^{Q}_{Q} &= 2Y_q Y_q^\dagger-\frac{3}{2}g_2^2-\frac{1}{12}g_{B-L}^2-\frac{8}{3}g_3^2\,;\\ \gamma^{Q^c}_{Q^c} &= 2Y_q^\dagger Y_q-\frac{3}{2}g_R^2-\frac{1}{12}g_{B-L}^2-\frac{8}{3}g_3^2\,;\\ \gamma^{\Phi}_{\Phi} &= \mathrm{tr}(3Y_qY_q^\dagger+Y_lY_l^\dagger)-\frac{3}{2}g_R^2-\frac{3}{2}g_2^2\,;\\ \gamma^{\bar\delta}_{\bar\delta} &= \frac{1}{2}\mathrm{tr}(Y_NY_N^\dagger)-4g_R^2-3g_{B-L}^2\,.\end{aligned} \tag{A.14}$$

Here we have continued to use g_2 for the $SU(2)_L$ coupling, and denoted the $SU(2)_R$ coupling with g_R. Eqs.(A.14) are consistent with [42], taking the appropriate normalization.

A.1.4 Region IV

$$\beta_{g_a}=(15,2,6,0)\ \text{ for } a=(1_{B-L},2_L,2_R,3_C)\,. \tag{A.15}$$

Since the new massive fields becoming active in this energy range are singlets under $U(1)_{B-L}\times SU(2)_R\times SU(2)_L$, only the running of the $SU(3)_C$ group changes. Moreover, the Yukawa coupling beta functions are those of Region III.

A.1.5 Region V

$$\beta_{g_a}=(42,42,34)\ \text{ for } a=(2_L,2_R,4_C)\,. \tag{A.16}$$

Since many new fields become active at $Q\geq M_C$, all gauge $\beta-$functions increase quite dramatically. In GUT normalization, $g_{B-L}=g_3=g_4$, where g_4 is the $SU(4)_C$ gauge coupling; this explains the entries in the last row of Table 2, with $\frac{194}{5}=\frac{3}{5}\cdot 42+\frac{2}{5}\cdot 34$.

No new Yukawa couplings appear in this energy range; instead, the couplings Y_q and Y_l get unified into the single coupling Y. At the same time, all MSSM matter superfields are

now in F or F^c introduced in Eq.(9); the D symmetry ensures that the anomalous dimensions of these two superfields are the same. Moreover, the $SU(2)_R$ triplet Higgs superfield $\bar{\delta}$ gets embedded into the much larger representation $\overline{\Sigma}_R$, and the $D-$partner $\overline{\Sigma}_L$ also appears, with identical anomalous dimensions.

Therefore Eqs.(A.13) change to

$$\begin{aligned} \beta_Y &= Y(\gamma_F^F + \gamma_\Phi^\Phi) + \gamma_F^F Y\,; \\ \beta_{Y_N} &= Y_N(\gamma_F^F + \gamma_{\overline{\Sigma}_R}^{\overline{\Sigma}_R}) + \gamma_F^F Y_N\,. \end{aligned} \tag{A.17}$$

The anomalous dimensions appearing in Eqs.(A.17) are:

$$\begin{aligned} \gamma_F^F &= 2Y^\dagger Y + \frac{15}{4}Y_N^\dagger Y_N - \frac{3}{2}g_R^2 - \frac{15}{4}g_4^2\,; \\ \gamma_\Phi^\Phi &= \mathrm{tr}(4YY^\dagger) - \frac{3}{2}g_R^2 - \frac{3}{2}g_2^2\,; \\ \gamma_{\overline{\Sigma}_R}^{\overline{\Sigma}_R} &= \frac{1}{2}\mathrm{tr}(Y_N Y_N^\dagger) - 4g_R^2 - 9g_4^2\,. \end{aligned} \tag{A.18}$$

A.2 Soft SUSY-breaking Parameters

We write the part of the Lagrangian that softly breaks supersymmetry as

$$\mathcal{L}_{SB} = -\frac{1}{6}h^{ijk}\phi_i\phi_j\phi_k - \frac{1}{2}b^{ij}\phi_i\phi_j - \frac{1}{2}(m^2)_i^j\phi^{*i}\phi_j - \frac{1}{2}M_a\lambda_a\lambda_a + h.c. \tag{A.19}$$

We assume universal boundary conditions,

$$\begin{aligned} h^{ijk} &= Y^{ijk}A_0\,; \\ (m^2)_i^j &= m_0^2\delta_i^j\,; \\ M_a &= M_{1/2}\ \forall a\,, \end{aligned} \tag{A.20}$$

which hold at scale $Q = M_X$. Here Y^{ijk} are the superpotential couplings introduced in Eq.(A.2).

The $\beta-$functions of the soft breaking parameters are defined by

$$\begin{aligned} \frac{d}{dt}h^{ijk} &= \frac{1}{16\pi^2}\beta_h^{ijk}\,; \\ \frac{d}{dt}b^{ij} &= \frac{1}{16\pi^2}\beta_b^{ij}\,; \\ \frac{d}{dt}(m^2)_i^j &= \frac{1}{16\pi^2}\beta_{m^2}{}_i^j\,; \\ \frac{d}{dt}M_a &= \frac{1}{16\pi^2}2g_a^2M_a^2\beta_{g_a}\,. \end{aligned} \tag{A.21}$$

Here β_{g_a} are the coefficients of the gauge $\beta-$functions introduced in Eq.(A.1). The other

$\beta-$functions appearing in Eqs.(A.21) can be written as*

$$\begin{aligned}
\beta_h^{ijk} &= \frac{1}{2}h^{ijl}Y_{lmn}Y^{mnk} + Y^{ijl}Y_{lmn}h^{mnk} - 2(h^{ijk} - 2M_aY^{ijk})g_a^2C_a(k) + (k \leftrightarrow i) + (k \leftrightarrow j)\,; \\
\beta_b^{ij} &= \frac{1}{2}b^{il}Y_{lmn}Y^{mnj} + +\mu^{il}Y_{lmn}h^{mnj} - 2(b^{ij} - 2M_a\mu^{ij})g_a^2C_a(i) + (i \leftrightarrow j)\,; \\
\beta_{m^2}{}_i^j &= \frac{1}{2}Y_{ipq}Y^{pqn}(m^2)_n^j + \frac{1}{2}Y^{jpq}Y_{pqn}(m^2)_i^n + 2Y_{ipq}Y^{jpr}(m^2)_r^q + h_{ipq}h^{jpq} \\
&- 8\delta_i^jM_aM_a^\dagger g_a^2C_a(i) + 2g_a^2(\mathbf{t}_a^A)_i^j\mathrm{tr}(\mathbf{t}_a^Am^2)\,. \qquad \text{(A.22)}
\end{aligned}$$

The last term in β_{m^2} can be nonzero only for $U(1)$ group factors. In the case at hand it is therefore either proportional to

$$S_Y = m_{H_u}^2 - m_{H_d}^2 + \mathrm{tr}[m_Q^2 - m_L^2 - 2m_u^2 + m_d^2 + m_e^2] \qquad \text{(A.23)}$$

or to

$$S_{B-L} = \frac{1}{2}(6m_{\overline{\Sigma}}^2 - 6m_\Sigma^2 + \mathrm{tr}[2m_Q^2 - 2m_{Q^c}^2 - 2m_L^2 + 2m_{L^c}^2])\,. \qquad \text{(A.24)}$$

For better readability, in Eqs.(A.23) and (A.24), as well as in subsequent equations, we have omitted the tildes on the subscripts of the squared scalar soft breaking masses; moreover, we use m_Σ and $m_{\overline{\Sigma}}$ for the soft mass of whatever parts of the original Σ and $\overline{\Sigma}$ superfields are active in a given energy range. Note that both S_Y and S_{B-L} evolve homogeneously. Since the boundary condition (A.20) for scalar soft breaking masses implies $S_Y = S_{B-L} = 0$ at scale M_X, they vanish at all scales. For completeness we nevertheless list these contributions in the following.

We are now ready to give explicit expressions for the soft breaking $\beta-$functions in the energy regions defined above.

A.2.1 Region I

Here the RGE are those of the MSSM [43]:

$$\begin{aligned}
\beta_{h_u} &= h_u\left[\mathrm{tr}(3Y_uY_u^\dagger) + 5Y_uY_u^\dagger + Y_d^\dagger Y_d - \frac{16}{3}g_3^2 - 3g_2^2 - \frac{13}{15}g_1^2\right] \\
&+ Y_u\left[\mathrm{tr}(6h_uY_u^\dagger) + 4h_uY_u^\dagger + 2Y_d^\dagger h_d + \frac{32}{3}g_3^2M_3 + 6g_2^2M_2 + \frac{26}{15}g_1^2M_1\right]\,; \\
\beta_{h_d} &= h_d\left[\mathrm{tr}(3Y_dY_d^\dagger + Y_eY_e^\dagger) + 5Y_dY_d^\dagger + Y_u^\dagger Y_u - \frac{16}{3}g_3^2 - 3g_2^2 - \frac{7}{15}g_1^2\right] \\
&+ Y_d\left[\mathrm{tr}(6h_dY_d^\dagger + 2h_eY_e^\dagger) + 4Y_d^\dagger h_d + 2Y_u^\dagger h_u + \frac{32}{3}g_3^2M_3 + 6g_2^2M_2 + \frac{14}{15}g_1^2M_1\right]\,: \\
\beta_{h_e} &= h_e\left[\mathrm{tr}(3Y_dY_d^\dagger + Y_eY_e^\dagger) + 5Y_e^\dagger Y_e - 3g_2^2 - \frac{9}{5}g_1^2\right] \\
&+ Y_e\left[\mathrm{tr}(6h_dY_d^\dagger + 2h_eY_e^\dagger) + 4Y_e^\dagger h_e + 6g_2^2M_2 + \frac{18}{5}g_1^2M_1\right]\,. \qquad \text{(A.25)}
\end{aligned}$$

*We suppress terms that can be nonzero only in the presence of complete gauge singlet chiral superfields.

$$
\begin{aligned}
\beta_B &= B\left[\mathrm{tr}(3Y_uY_u^\dagger + 3Y_dY_d^\dagger + Y_eY_e^\dagger) - 3g_2^2 - \frac{3}{5}g_1^2\right] \\
&+ \mu\left[\mathrm{tr}(6h_uY_u^\dagger + 6h_dY_d^\dagger + 2h_eY_e^\dagger) + 6g_2^2M_2 + \frac{6}{5}g_1^2M_1\right] . \qquad \text{(A.26)}
\end{aligned}
$$

$$
\begin{aligned}
\beta_{m_{H_u}^2} &= 6\mathrm{tr}\left[(m_{H_u}^2 + m_Q^2)Y_u^\dagger Y_u + Y_u^\dagger m_u^2 Y_u + h_u^\dagger h_u\right] - 6g_2^2|M_2|^2 - \frac{6}{5}g_1^2|M_1|^2 + \frac{3}{5}g_1^2S_Y\,; \\
\beta_{m_{H_d}^2} &= \mathrm{tr}\left[6(m_{H_d}^2 + m_Q^2)Y_d^\dagger Y_d + 6Y_d^\dagger m_d^2 Y_d + 2(m_{H_d}^2 + m_L^2)Y_e^\dagger Y_e + 2Y_e^\dagger m_e^2 Y_e\right. \\
&\quad \left. + 6h_d^\dagger h_d + 2h_e^\dagger h_e\right] - 6g_2^2|M_2|^2 - \frac{6}{5}g_1^2|M_1|^2 - \frac{3}{5}g_1^2S_Y\,; \\
\beta_{m_Q^2} &= (m_Q^2 + 2m_{H_u}^2)Y_u^\dagger Y_u + (m_Q^2 + 2m_{H_d}^2)Y_d^\dagger Y_d + [Y_u^\dagger Y_u + Y_d^\dagger Y_d]m_Q^2 + 2Y_u^\dagger m_u^2 Y_u \\
&+ 2Y_d^\dagger m_d^2 Y_d + 2h_u^\dagger h_u + 2h_d^\dagger h_d - \frac{32}{3}g_3^2|M_3|^2 - 6g_2^2|M_2|^2 - \frac{2}{15}g_1^2|M_1|^2 - \frac{1}{5}g_1^2S_Y\,; \\
\beta_{m_L^2} &= (m_L^2 + 2m_{H_d}^2)Y_e^\dagger Y_e + 2Y_e^\dagger m_e^2 Y_e + Y_e^\dagger Y_e m_L^2 + 2h_e^\dagger h_e - 6g_2^2|M_2|^2 - \frac{6}{5}g_1^2|M_1|^2 - \frac{3}{5}g_1^2S_Y\,; \\
\beta_{m_u^2} &= (2m_u^2 + 4m_{H_u}^2)Y_uY_u^\dagger + 4Y_um_Q^2Y_u^\dagger + 2Y_uY_u^\dagger m_u^2 + 4h_uh_u^\dagger - \frac{32}{3}g_3^2|M_3|^2 - \frac{32}{15}g_1^2|M_1|^2 \\
&- \frac{4}{5}g_1^2S_Y\,; \\
\beta_{m_d^2} &= (2m_d^2 + 4m_{H_d}^2)Y_dY_d^\dagger + 4Y_dm_Q^2Y_d^\dagger + 2Y_dY_d^\dagger m_d^2 + 4h_dh_d^\dagger - \frac{32}{3}g_3^2|M_3|^2 - \frac{8}{15}g_1^2|M_1|^2 \\
&+ \frac{2}{5}g_1^2S_Y\,; \\
\beta_{m_e^2} &= (2m_e^2 + 4m_{H_d}^2)Y_eY_e^\dagger + 4Y_em_L^2Y_e^\dagger + 2Y_eY_e^\dagger m_e^2 + 4h_eh_e^\dagger - \frac{24}{5}g_1^2|M_1|^2 + \frac{6}{5}g_1^2S_Y\,. \qquad \text{(A.27)}
\end{aligned}
$$

A.2.2 Region II

Most expression from Region I remain form–invariant; however, the Yukawa couplings should now be interpreted as the high–scale couplings $Y_{f,1}$ rather than as low–scale (MSSM) couplings Y_f. In addition, the beta–function for the $SU(2)_L$ singlet slepton mass changes, and we have to introduce beta–function for $m_{\overline{\Sigma}}$ as well as h_N:

$$
\begin{aligned}
\beta_{h_N} &= h_N[\frac{1}{2}\mathrm{tr}(Y_N^\dagger Y_N) + 4Y_eY_e^\dagger + 2Y_NY_N^\dagger - \frac{36}{5}g_1^2] \\
&+ Y_N[Y_N^\dagger h_N + 8Y_e^\dagger h_e + 4Y_N^\dagger h_N + \frac{72}{5}g_1^2|M_1|^2]\,. \qquad \text{(A.28)}
\end{aligned}
$$

$$
\beta_{B_\Sigma} = B_\Sigma[\frac{1}{2}\mathrm{tr}(Y_NY_N^\dagger) - \frac{48}{5}g_1^2] + M_\Sigma[\mathrm{tr}0(Y_N^\dagger h_N) + \frac{96}{5}g_1^2|M_1|^2]\,. \qquad \text{(A.29)}
$$

$$
\begin{aligned}
\beta_{m_e^2} &= (2m_e^2 + 4m_{H_d}^2)Y_eY_e^\dagger + 4Y_em_L^2Y_e^\dagger + 2Y_eY_e^\dagger m_e^2 + m_e^2Y_NY_N^\dagger + 2Y_N^\dagger m_e^2Y_N \\
&+ Y_NY_N^\dagger m_e^2 + 2Y_N^\dagger m_{\overline{\Sigma}}^2 Y_N + (4m_e^2 + 2m_{\overline{\Sigma}}^2)Y_NY_N^\dagger + 4h_eh_e^\dagger + 2h_Nh_N^\dagger \\
&- \frac{24}{5}g_1^2|M_1|^2 + \frac{6}{5}g_1^2S_Y\,; \\
\beta_{m_{\overline{\Sigma}}^2} &= \mathrm{tr}[\frac{1}{2}Y_N^\dagger Y_N m_{\overline{\Sigma}}^2 + 2Y_N^\dagger m_e^2 Y_N + \frac{1}{2}Y_NY_N^\dagger m_{\overline{\Sigma}}^2] + h_Nh_N^\dagger - \frac{96}{5}g_1^2|M_1|^2 + \frac{12}{5}g_1^2S_Y \qquad \text{(A.30)}
\end{aligned}
$$

M_Σ appearing in the Eq.(A.29) is the supersymmetric Σ and $\overline{\Sigma}$ mass, which comes from a term $M_\Sigma \Sigma\overline{\Sigma}$ in the superpotential. Note that to one–loop order B_Σ does not appear on the right–hand side of any other RGE, hence it has no impact on the low–energy spectrum. We nevertheless list its RGE for completeness; it might be relevant, e.g., for the detailed dynamics of intermediate–scale symmetry breaking, which we here merely parameterize through the vev σ.

A.2.3 Regions III and IV

Here the number of independent parameters diminishes: $SU(2)_R$ invariance implies $m_d = m_u \equiv m_{Q^c}$, $m_e = m_N \equiv m_{L^c}$, $m_{H_u} = m_{H_d} \equiv m_\Phi$, $h_u = h_d \equiv h_q$ and $h_e = h_N \equiv h_l$ at energies $\geq M_R$:

$$\begin{aligned}
\beta_{h_q} &= h_q \left[\mathrm{tr}(3Y_q Y_q^\dagger + Y_l Y_l^\dagger) + 5 Y_q Y_q^\dagger + Y_q^\dagger Y_q - \frac{16}{3} g_3^2 - 3 g_2^2 - 3 g_R^2 - \frac{g_{B-L}^2}{6} \right] \\
&+ Y_q \left[\mathrm{tr}(6 h_q Y_q^\dagger + 2 h_l Y_l^\dagger) + 4 h_q Y_q^\dagger + 2 Y_q^\dagger h_q + \frac{32}{3} g_3^2 M_3 + 6 g_2^2 M_2 + 6 g_R^2 M_R + \frac{g_{B-L}^2}{3} M_{B-L} \right] ; \\
\beta_{h_l} &= h_l \left[\mathrm{tr}(3 Y_q Y_q^\dagger + Y_l Y_l^\dagger) + 5 Y_l Y_l^\dagger + Y_l^\dagger Y_l + \frac{3}{2} Y_N^\dagger Y_N - 3 g_2^2 - 3 g_R^2 - \frac{3}{2} g_{B-L}^2 \right] \\
&+ Y_l \left[\mathrm{tr}(6 h_q Y_q^\dagger + 2 h_l Y_l^\dagger) + 4 h_l Y_l^\dagger + 2 Y_l^\dagger h_l + 3 Y_N^\dagger h_N + 6 g_2^2 M_2 + 6 g_R^2 M_R + 3 g_{B-L}^2 \right] ; \\
\beta_{h_N} &= h_N \left[\frac{1}{2} \mathrm{tr}(Y_N^\dagger Y_N) + 4 Y_l Y_l^\dagger + 3 Y_N Y_N^\dagger - 7 g_R^2 - \frac{9}{2} g_{B-L}^2 \right] \\
&+ Y_N \left[Y_N^\dagger h_N + 8 Y_l^\dagger h_l + 6 Y_N^\dagger h_N + 14 g_R^2 M_R + 9 g_{B-L}^2 \right] .
\end{aligned} \tag{A.31}$$

$$\begin{aligned}
\beta_B &= B \left[\mathrm{tr}(6 Y_q Y_q^\dagger + 2 Y_l Y_l^\dagger) - 3 g_2^2 - 3 g_R^2 \right] + \mu \left[\mathrm{tr}(12 h_q Y_q^\dagger + 4 h_l Y_l^\dagger) + 6 g_2^2 M_2 + 6 g_R^2 M_R \right] ; \\
\beta_{B_\Sigma} &= B_\Sigma \left[\frac{1}{2} \mathrm{tr}(Y_N Y_N^\dagger) - 8 g_R^2 - 6 g_{B-L}^2 \right] + M_\Sigma \left[\mathrm{tr}(Y_N^\dagger h_N) + 16 g_R^2 M_R + 12 g_{B-L}^2 M_{B-L} \right] .
\end{aligned} \tag{A.32}$$

$$
\begin{aligned}
\beta_{m_\Phi^2} &= \mathrm{tr}\Big[6(m_\Phi^2+m_Q^2)Y_q^\dagger Y_q + 6Y_q^\dagger m_{Q^c}^2 Y_q + 2(m_\Phi^2+m_L^2)Y_l^\dagger Y_l + 2Y_l^\dagger m_{L^c}^2 Y_l \\
&\quad +6h_q^\dagger h_q + 2h_l^\dagger h_l\Big] - 6g_2^2|M_2|^2 - 6g_R^2|M_R|^2\,; \\
\beta_{m_\Sigma^2} &= \frac{1}{2}\mathrm{tr}(Y_N^\dagger Y_N m_{\overline{\Sigma}}^2 + Y_N Y_N^\dagger m_\Sigma^2) + \mathrm{tr}(2Y_N^\dagger m_{L^c}^2 Y_N + h_N^\dagger h_N) \\
&- 16|M_R|^2 g_R^2 - 12|M_{B-L}|^2 g_{B-L}^2 + 3g_{B-L}^2 S_{B-L}\,; \\
\beta_{m_{\overline{\Sigma}}^2} &= -16|M_R|^2 g_R^2 - 12|M_{B-L}|^2 g_{B-L}^2 - 3g_{B-L}^2 S_{B-L}\,; \\
\beta_{m_Q^2} &= 2(m_Q^2+2m_\Phi^2)Y_q^\dagger Y_q + 2Y_q^\dagger Y_q m_Q^2 + 4Y_q^\dagger m_{Q^c}^2 Y_q \\
&+ 4h_q^\dagger h_q - \frac{32}{3}g_3^2|M_3|^2 - 6g_2^2|M_2|^2 - \frac{1}{3}g_{B-L}^2|M_{B-L}|^2 + \frac{1}{2}g_{B-L}^2 S_{B-L}\,; \\
\beta_{m_L^2} &= 2(m_L^2+2m_\Phi^2)Y_l^\dagger Y_l + 2Y_l^\dagger Y_l m_L^2 + 4Y_l^\dagger m_l^2 Y_l \\
&+ 4h_l^\dagger h_l - 6g_2^2|M_2|^2 - 3g_{B-L}^2|M_{B-L}|^2 - \frac{3}{2}g_{B-L}^2 S_{B-L}\,; \\
\beta_{m_{Q^c}^2} &= (2m_{Q^c}^2+4m_\Phi^2)Y_q Y_q^\dagger + 4Y_q m_Q^2 Y_q^\dagger + 2Y_q Y_q^\dagger m_{Q^c}^2 + 4h_q h_q^\dagger \\
&- \frac{32}{3}g_3^2|M_3|^2 - 6g_R^2|M_R|^2 - \frac{1}{3}g_{B-L}^2|M_{B-L}|^2 - \frac{1}{2}g_{B-L}^2 S_{B-L}\,; \\
\beta_{m_{L^c}^2} &= (2m_{L_c}^2+4m_\Phi^2)Y_l Y_l^\dagger + 4Y_l m_L^2 Y_l^\dagger + 2Y_l Y_l^\dagger m_{L^c}^2 + 4h_l h_l^\dagger + \frac{3}{2}m_{L^c}^2 Y_N Y_N^\dagger + \frac{3}{2}Y_N Y_N^\dagger m_{L^c}^2 \\
&+ 3Y_N^\dagger m_{L^c}^2 Y_N + 3Y_N^\dagger m_{\overline{\Sigma}}^2 Y_N + 3h_N^\dagger h_N - 6g_R^2|M_R|^2 - 3g_{B-L}^2|M_{B-L}|^2 + \frac{3}{2}g_{B-L}^2 S_{B-L}\,.
\end{aligned}
\tag{A.33}
$$

Note that Σ, which we introduced to allow a $D-$flat direction for symmetry breaking at scale M_R, does not have any superpotential couplings, hence its soft mass does not appear in any of the other RGE. We again list its RGE for completeness.

A.2.4 Region V

At scales above M_C the spectrum further simplifies: G_{422} invariance implies that $m_Q = m_L \equiv m_F$, $m_{Q^c} = m_{L^c} = m_{F^c}$, and $h_q = h_l \equiv h$. In addition, the discrete D symmetry implies $m_{\overline{\Sigma}_L} = m_{\overline{\Sigma}_R} \equiv m_{\overline{\Sigma}}$ and $m_F = m_{F^c}$:

$$
\begin{aligned}
\beta_h &= h\left[4\mathrm{tr}(YY^\dagger) + \frac{15}{4}Y_N Y_N^\dagger + 5YY^\dagger + Y^\dagger Y - \frac{15}{2}g_4^2 - 3g_2^2 - 3g_R^2\right] \\
&+ Y\left[\mathrm{tr}(8hY^\dagger) + \frac{15}{2}h_N Y_N^\dagger + 4hY^\dagger + 2Y^\dagger h + 15g_4^2 M_4 + 6g_2^2 M_2 + 6g_R^2 M_R\right]\,; \\
\beta_{h_N} &= h_N\left[\frac{1}{2}\mathrm{tr}(Y_N^\dagger Y_N) + 4YY^\dagger + \frac{15}{2}Y_N Y_N^\dagger - \frac{33}{2}g_4^2 - 7g_R^2\right] \\
&+ Y_N\left[\mathrm{tr}(h_N Y_N^\dagger) + 8Y^\dagger h + 15Y_N^\dagger h_N + 33g_4^2 M_4 + 14g_R^2 M_R\right]\,.
\end{aligned}
\tag{A.34}
$$

$$
\begin{aligned}
\beta_B &= B\left[\mathrm{tr}(8YY^\dagger) - 3g_2^2 - 3g_R^2\right] + \mu\left[\mathrm{tr}(16hY^\dagger) + 6g_2^2 M_2 + 6g_R^2 M_R\right]\,; \\
\beta_{B_\Sigma} &= B_\Sigma\left[\frac{1}{2}\mathrm{tr}(Y_N Y_N^\dagger) - 8g_R^2 - 18g_4^2\right] + m_\Sigma\left[\mathrm{tr}(Y_N^\dagger h_N) + 16g_R^2 M_R + 36g_4^2 M_4\right]\,.
\end{aligned}
\tag{A.35}
$$

$$
\begin{aligned}
\beta_{m_\Phi^2} &= \mathrm{tr}\left[8(m_\Phi^2+m_F^2)Y^\dagger Y + 8Y^\dagger m_F^2 Y + 8h_u^\dagger h_u\right] - 6g_2^2|M_2|^2 - 6g_R^2|M_R|^2\,; \\
\beta_{m_\Sigma^2} &= \frac{1}{2}\mathrm{tr}(Y_N^\dagger Y_N m_{\overline{\Sigma}}^2 + Y_N Y_N^\dagger m_{\overline{\Sigma}}^2) + \mathrm{tr}(2Y_N^\dagger m_F^2 Y_N + h_N^\dagger h_N) - 16|M_R|^2 g_R^2 - 36|M_4|^2 g_4^2\,; \\
\beta_{m_{\overline{\Sigma}}^2} &= -16|M_R|^2 g_R^2 - 36|M_4|^2 g_4^2\,; \\
\beta_{m_F^2} &= 2(m_F^2+2m_\Phi^2)Y^\dagger Y + 2Y^\dagger Y m_F^2 + \frac{15}{4}(m_F^2+2m_{\overline{\Sigma}}^2)Y_N Y_N^\dagger + \frac{15}{4}Y_N Y_N^\dagger m_F^2 \\
&+ \frac{15}{2}Y_N m_F^2 Y_N^\dagger + \frac{15}{2}h_N h_N^\dagger + 4Y^\dagger m^2 F Y + 4h^\dagger h - 15g_4^2|M_4|^2 - 6g_2^2|M_2|^2\,. \qquad \text{(A.36)}
\end{aligned}
$$

References

[1] H. Fritzsch and P. Minkowski, Ann. Phys. **93** (1975) 193; M.S. Chanowitz, J. Ellis and M.K. Gaillard, Nucl. Phys. **B129** (1977) 506.

[2] H. Georgi and D. V. Nanopoulos, Nucl. Phys. B **155** (1979) 52; T.E. Clark, T.K. Kuo and N. Nakagawa, Phys. Lett. B **115** (1982) 26.

[3] P. Minkowski, Phys. Lett. B **67** (1977) 421.

[4] M. Fukugita and T. Yanagida, Phys. Lett. B **174** (1986) 45.

[5] J. C. Pati and A. Salam, Phys. Rev. D. **10** (1974) 275.

[6] B. Aharmim et al. [SNO Collab.], Phys. Rev. C **72** (2005) 055502.

[7] Y. Ashie et al. [Super-Kamiokande Collab.], Phys. Rev. D **71** (2005) 112005.

[8] T. Araki et al. [KamLAND Collaboration], Phys. Rev. Lett. **94** (2005) 081801.

[9] C.S. Aulakh, B. Bajc, A. Melfo, A. Rasin and G. Senjanovic, Nucl. Phys. **B597** (2001) 89.

[10] For introductions to supersymmetry in general, and to mSUGRA in particular, see e.g. M. Drees, R.M. Godbole and P. Roy, *Theory and Phenomenology of Sparticles*, World Scientific (2004); H. Baer and X. Tata, *Weak scale supersymmetry: From superfields to scattering events*, Cambridge, UK University Press (2006).

[11] C.S. Aulakh, B. Bajc, A. Melfo, A. Rasin and G. Senjanovic, Phys. Lett. **B460** (1999) 325.

[12] For recent analyses, see M.E. Gomez, T. Ibrahim, P. Nath and S. Skadhauge, Phys. Rev. **D72** (2005) 095008; W. Altmannshofer, D. Guadagnoli, S. Raby and D.M. Straub, `arXiv:0801.4363 [hep-ph]`; H. Baer, S. Kraml, S. Sekmen and H. Summy, JHEP **0803** (2008) 056.

[13] U. Amaldi, W. de Boer and H. Fürstenau, Phys. Lett. **B260** (1991) 447; P. Langacker and M.-x. Luo, Phys. Rev. **D44** (1991) 817; J.R. Ellis, S. Kelley and D.V. Nanopoulos, Phys. Lett. **B260** (1991) 131; C. Giunti, C.W. Kim and U.W. Lee, Mod. Phys. Lett. **A6** (1991) 1745.

[14] See e.g. A. Djouadi, M. Drees and J.-L. Kneur, JHEP **0603** (2006) 033; J.R. Ellis, S. Heinemeyer, K.A. Olive, A.M. Weber and G. Weiglein, JHEP **0708** (2007) 083; and references therein.

[15] B.C. Allanach, Comput. Phys. Commun. **143** (2002) 305-331.

[16] D.M. Pierce, J.A. Bagger, K.T. Matchev and R.-j. Zhang, Nucl. Phys. **B491** (1997) 3.

[17] L.E. Ibáñez and G.G. Ross, Phys. Lett. **110B**, 215 (1982); L.E. Ibáñez, Phys. Lett. **118B**, 73 (1982); J. Ellis, D.V. Nanopoulos and K. Tamvakis, Phys. Lett. **121B**, 123 (1983); L. Alvarez-Gaumé, J. Polchinski and M.B. Wise, Nucl. Phys. **B221**, 495 (1983).

[18] G. Bélanger, F. Boudjema, A. Pukhov and A. Semenov, Comput. Phys. Commun. **149** (2002) 103, `hep--ph/0112278`, and Comput. Phys. Commun. **174** (2006) 577, `hep--ph/0405253`.

[19] Particle Data Group, W.M. Yao et al., J. Phys. G. **33** (2006) 1.

[20] B.C. Allanach, A. Djouadi, J.L. Kneur, W. Porod and P. Slavich, JHEP **0409** (2004) 044; S. Heinemeyer, W. Hollik and G. Weiglein, Phys. Rept. **425** (2006) 265.

[21] S. Bertolini, F. Borzumati and A. Masiero, Phys. Lett. **B192** (1987) 437, and Nucl. Phys. **B294** (1987) 321.

[22] Heavy Flavor Averaging Group (HFAG), `hep--ex/0704.3575`.

[23] F. Borzumati, C. Greub, T. Hurth and D. Wyler, Phys. Rev. D. **62** (2000) 075005.

[24] L.L. Everett, G.L. Kane, S. Rigolin, L.-T. Wang and T.T. Wang, JHEP **0201** (2002) 022.

[25] K.-i. Okumura and L. Roszkowski, Phys. Rev. Lett. **92** (2004) 161801.

[26] G. Degrassi, P. Gambino and G.F. Giudice, JHEP. **0012** (2000) 009.

[27] S. Bertolini, F. Borzumati, A. Masiero and G. Ridolfi, Nucl. Phys. **B353** (1991) 591.

[28] J.P. Miller, E. de Rafael, and B.L. Roberts, Rept. Prog. Phys. **70** (2007) 795.

[29] See e.g. E.W. Kolb and M.S. Turner, *The Early Universe*, Westview Press (1994).

[30] D.N. Spergel et al. [WMAP Collab.], Astrophys. J. Suppl. **170** (2007) 377.

[31] J. Dunkley et al. [WMAP Collab.], arXiv:0803.0586 [astro-ph].

[32] D0 Collab. and CDF collab, M.H.L.S. Wang et al., `hep--ex/0705.3873`.

[33] P. Langacker and N. Polonsky, Phys. Rev. D.**47** (1993) 4028.

[34] L. Calibbi, Y. Mambrini, and S.K. Vempati, JHEP **0709** (2007) 081.

[35] J.R. Ellis, T. Falk and K.A. Olive, Phys. Lett. **B444** (1998) 367; M.E. Gomez, G. Lazarides and C. Pallis, Phys. Lett. **B487** (2000) 313; J.R. Ellis, T. Falk, K.A. Olive and M. Srednicki, Astropart. Phys. **13** (2000) 181, Erratum-ibid. **15** (2001) 413.

[36] M. Drees, Phys. Lett. B **181** (1986) 279.

[37] J.L. Feng, K.T. Matchev and T. Moroi, Phys. Rev. Lett. **84** (2000) 2322, and Phys. Rev. **D61** (2000) 75005.

[38] See e.g. ATLAS collab., ATLAS Technical Design Report, CERN/LHCC/99-14, Ch. 14.

[39] J. Edsjö and P. Gondolo, Phys. Rev. **D56** (1997) 1879.

[40] M. Drees and M.M. Nojiri, Phys. Rev. **D47** (1997) 376; T. Falk, R. Madden, K.A. Olive and M. Srednicki, Phys. Lett. **B318** (1993) 354.

[41] S.P. Martin and M.T. Vaughn, Phys. Rev. D**50** (1994) 2282.

[42] N. Setzer and S. Spinner, Phys. Rev. D**71** (2005) 115010.

[43] N.K. Falck, Z. Phys. **C30**, 247 (1986).